DISSECTING THE ROLE OF KINASE ISOFORMS USING NEW TOOLS FOR ACTIVATION AND INACTIVATION OF KINASES *IN VIVO*

Pei-Hsuan Chu

A dissertation submitted to the faculty of the University of North Carolina at Chapel Hill in partial fulfillment of the requirements for the degree of Doctor of Philosophy in the department of Pharmacology.

Chapel Hill
2013

Approved by:
Klaus M. Hahn
Keith Burridge
Adrienne D. Cox
Lee M. Graves
T. Kendall Harden

ABSTRACT

Pei-Hsuan Chu: Dissecting the role of kinase isoforms using new tools for activation and inactivation of kinases *in vivo*
(Under the direction of Dr. Klaus M. Hahn)

The Src family kinases (SFKs) are comprised of nine highly homologous members that participate in various signaling pathways, to regulate events such as proliferation, differentiation, cell migration, adhesion, and survival. While Src has been intensively studied, less is known about other family members. Unfortunately, similarities in the structure and regulation of SFKs have made it difficult to dissect their unique functions. Differential expression of individual SFKs have been found in various cancer cell lines, yet their functional specificity remains largely unknown. Previous strategies to investigate SFK specificity, such as overexpression and use of non-selective inhibitors, have been hampered by genetic compensation or lack of specificity. Therefore, it was imperative that new tools be developed in order to identify specific roles for individual SFKs. This dissertation describes two strategies to manipulate the activity of SFKs and to reveal novel information about their functional specificity in cell motility. The first study I performed used a small molecule to specifically activate each SFK isoform and to elucidate possible mechanisms contributing to the distinct activation phenotypes of Src and a Src family member, Fyn. In this study, new computational methods were developed to automatically analyze the dynamics of morphological changes. In the second study, I used light to manipulate Src activity. These

strategies not only provide absolute control of specific Src family members, but also allow for spatial control of kinase activity. Additionally, these strategies utilize the same conserved site in the catalytic domain of the kinase and can be broadly applied to other tyrosine kinases.

DEDICATION

To my dear husband, Hsuan-Hao Wang and my lovely son, Zachary Wang,

Your love is what kept me moving forward.

ACKNOWLEDGEMENTS

First, I would like to express my deepest appreciation to my advisor, Dr. Klaus M. Hahn, for his excellent guidance, caring, and for providing me with abundant resources for doing research. I would like to thank my committee members, Keith Burridge, Adrienne Cox, Lee Graves, and Kendall Harden for their time and insightful comments; they made this a better project. I would also like to thank Andrei Karginov, who has been my second mentor on this project, for his patience and inspiration. I would like to thank my collaborator, Denis Tsygankov, who put so much effort into developing new methods to push this project to the next level. I can't thank them enough.

To the Hahn lab members, all past and present, thank you for your inspiration and warmth in both science and daily life. I am very grateful to Dan Marston, Kim Marston, Ellen O'Shaughnessy, Scott Slattery, Onur Dagliyan, and Chris Welch, for helping me prepare my thesis and defense.

I would also like to thank Dr. Darrel Stafford for giving me the chance to work in his lab, and for encouraging me to pursue my PhD at UNC. Last, I would like to thank my friends and family who have been very supportive through all these years. I would especially like to thank my parents, Jen-Hsiang Chu and Hui-Fen Shen for their unconditional love, and my parents-in-law, Chen-Wen Wang and Hsueh-Jung Hsu, for being so caring and fully supportive.

TABLE OF CONTENTS

LIST OF FIGURES

LIST OF ABBREVIATIONS

ATP	Adenosine Triphosphate
BSA	Bovine Serum Albumin
CA	Constitutively Active
COS-7 cell	Fibroblast-like cell line derived from monkey kidney tissue
DHFR	Dihydrofolate Reductase
DMEM	Dulbecco's Modified Eagle Medium
dNTP	Deoxyribonucleotide Triphosphate
c-Src	Proto-Oncogene Encoded Src Tyrosine Kinase
ECFP	Enhanced Cyan Fluorescent Protein
EGFP	Enhanced Green Fluorescent Protein
FA	Focal Adhesion
FAK	Focal Adhesion Kinase
FBS	Fetal Bovine Serum
FDA	Food and Drug Administration
FKBP	FK506 Binding Protein
GS	Glycine-Serine Amino Acid Sequence
GUI	Graphical User Interface
HRP	Horse Radish Peroxidase
IgG	Immunoglobulin G
iFKBP	insertable FKBP
KD	Kinase Dead Mutant

LOV	Light, Oxygen, and Voltage Domain
MSD	Mean Squared Displacement
Opti-MEM	Optimum Modified Eagle's Medium
PAS	Per-ARNT-Sim Core Domain
PCR	Polymerase Chain Reaction
P_{cr}	Polarization Critical Parameters
pH	Concentration of Hydrogen Ions
pTyr	Phosphotyrosine
Rap	Rapamycin
RapR	Rapamycin-Regulated
R_{cr}	Rate of Area Change Critical Parameters
SFK	Src Family Kinase
SH2	Src Homology 2 domain
SH3	Src Homology 3 domain
SH4	Src Homology 4 domain
Src CA	Constitutively Active Src
Src KD	Kinase-Dead Src
SYF	Mouse Embryonic Fibroblasts Deficient in Src, Yes, and Fyn
TIRF	Total Internal Reflection Microscopy
Tris	Tris(hydroxymethyl)aminomethane
v-Src	Src Tyrosine Kinase first identified in Rous Sarcoma Virus
ZDC	Zero-drift Compensation

CHAPTER ONE: INTRODUCTION

1.1 Introduction to Src family kinases

A historical perspective

In 1911, Peyton Rous first proposed that an agent separated from a malignant tumor growing on a chicken could cause infection by exposing it to a healthy bird (1). This finding implied that cancers could be transmitted through a virus, later known as the Rous sarcoma virus, an idea that was discredited by most experts in the field at the time. In the 1950s direct evidence demonstrated that virus particles were adequate to initiate tumor development (2). Additionally, part of the viral genome was reported to be required for the maintenance of the transformed phenotype of cells (3). The viral oncogene, *v-src*, was later identified and shown to be required for induction and maintenance of the transformation of infected cells (4-6). Src proteins are able to facilitate cell transformation via phosphorylation of target proteins (7). Src has been established as a tyrosine protein kinase (M.W. 60 kDa), first called $pp60^{v\text{-}src}$ and now known as v-Src (8). A homologous protein was identified in vertebrate cells as cellular Src (c-Src) (9-11), which was similar in structure and function to v-Src (12-17). c-Src differs in sequence from v-Src in its carboxyl terminus and exhibits relatively poor transforming potential (18). Therefore, the term proto-oncogene is used to describe c-Src, which emphasizes that the kinase does not possess transforming potential unless mutated or overexpressed.

1.2 The role of Src family kinases in cancer progression

Mutations have been found in v-Src, which alter various properties of the protein including its transforming potential. However, mutations are rarely found in c-Src. More commonly, elevated expression levels and increased catalytic activity of c-Src are found in human cancers. The fact that expression levels and activity of SFKs increase with the stage of disease, for example in colorectal cancer, provides strong evidence of the involvement of SFKs in cancer progression (19, 20). SFKs are over-expressed and over-activated in many human malignancies, including breast, colorectal, prostate, and lung cancers (21, 22). How do the SFKs contribute to cancer progression? Functional studies of SFKs suggest that they regulate a broad range of cellular processes, including proliferation, differentiation, migration, and angiogenesis (23). Src is thought to facilitate motility and invasion of tumor cells by transforming cell shapes (24, 25), promoting assembly and disassembly of focal adhesions (26-28), regulating expression of matrix metalloproteinases that are capable of degrading the extracellular matrix (29, 30), and activating angiogenesis signaling pathways (31). These cellular processes play essential roles in cancer initiation, survival, and eventually result in metastasis. Nearly a century after identification of Src, this protein still holds a prominent place in cancer research due to its diverse signaling roles in normal cell development and tumor progression (32-34).

The current U.S. Food and Drug Administration (FDA)-approved Src family kinase inhibitor, Dasatinib, has been used in the treatment of chronic myelogenous leukemia and Philadelphia chromosome-positive acute lymphoblastic leukemia. This inhibitor targets the ATP binding pocket of kinases and has been reported to inhibit Abl, c-Kit, ephrin receptors, and several other tyrosine kinases (35). In addition, recent studies suggest that inhibition by

targeting the kinase domain of Src may only be partially effective as its non-catalytic domain is still involved with integrin signaling (26). Moreover, SFKs not only play critical roles in cancer cells but also are important for normal cellular functions. Identification of SFK substrates in specific signaling events is essential to the development and application of clinically relevant biomarkers and inhibitors. Continued investigation to understand the signaling networks regulated by SFKs will provide a foundation for cancer research and drug development.

1.3 Functional specificity of Src family isoforms

Since the discovery of c-Src, intensive research has been performed to characterize its cellular functions and regulation. The Src family of kinases has nine family members including, Src, Fyn, Yes, Lyn, Lck, Hck, Blk, Fgr, and Yrk (23). While c-Src is the best-studied proto-oncogene, less is known about its family members. The high degree of similarity in structure and regulation suggests SFKs can partially compensate for each other *in vivo*. Indeed, knockout studies have shown that only mice deficient in all three genes (*src, yes*, and *fyn*) show embryonic lethality (36). Additionally, Roche *et al.* provided strong evidence that Src, Yes, and Fyn are functionally redundant during cell cycle progression (37). However, their distinct expression patterns and cellular distributions imply unique functions.

There is a growing interest in the functional specificity of each SFK, due to the findings that individual SFKs may contribute differently to different types of cancer. For example, Fyn is upregulated in prostate cancer as compared to other SFKs (38). Also, the expression of Fyn, but not Src, is correlated with pancreatic cancer metastasis (39). In

colorectal carcinoma, patients with elevated Yes activity have a more aggressive form of the disease and lower survival rates than patients with elevated Src activity (40). Lyn activity is significantly elevated in glioblastoma tumor cells and results in highly invasive phenotypes (41). Despite the different effects of individual SFKs on various types of cancer, the molecular mechanisms of individual SFKs contributing to distinct functions are largely unknown. It is important to understand how each Src family member is sending specific signals in different type of cancers. Therefore, the development of inhibitors that specifically target the disease-relevant SFK member, or pathways unique to them, will be valuable in cancer treatment.

1.4 Experimental approach to study the functions of Src family kinases

Overexpression or knockdown techniques are often used to study the function of genes of interest. However, these genetic alterations can fail to capture the phenotype since other genes can compensate for the loss of function. Moreover, it is impossible to assay immediate effects using this strategy. Various techniques have been developed to understand the direct cellular effects of Src activation. One approach is focused on identifying phosphorylated substrates of SFKs. In this approach, studies have used mutated kinases that have selectivity for radiolabeled ATP analogs, instead of natural ATPs, to identify the direct phosphorylated substrates of SFKs (42, 43). In addition, the kinase-substrate interactions of all SFKs (519 purified substrates) have been compared in the same platform using surface plasmon resonance (44). However, these methods were restricted to cell lysates or purified proteins. Disadvantages of these methods are the lack of information involving physiological

relevance and the failure to identify the substrate specificity contributed by cellular localization of kinases.

Other strategies have been employed to manipulate the activity of Src directly. One extensively used tool is temperature-sensitive v-Src (ts LA29) (45), which was generated via mutagenesis of the Prague strain of Rous sarcoma virus. This Src mutant is active at permissive temperatures (33-37°C) and becomes inactive when switching cells to a restrictive temperature (41°C). Src activity can also be manipulated via chemical rescue of mutant Src. The catalytic activity of mutant Src can be restored by the small molecule imidazole (46). However, there are caveats with these approaches: shifting temperature affects more than Src activity and the high concentrations of imidazole required for experiments cause toxicity in living cells. Additionally, the tools mentioned above are only designed to manipulate Src, not other SFK members. In the first part of this dissertation, I describe a new strategy I apply to gain absolute control of individual SFKs in a temporal manner for the first time. Using this strategy, catalytic activity of each SFK can be allosterically controlled with a cell permeable molecule. In the second part of this dissertation, I use light to gain spatio-temporal control of Src activity. These new tools are capable of dissecting out the unique functions of SFK members in dynamic events and make it possible to reveal the immediate functional consequences of specific kinase activation.

1.5 Structure and regulation of Src family kinases

SFKs share a similar domain arrangement: a Src homology 4 (SH4) domain, a Unique domain, followed by SH3, SH2 domains and a Tyrosine Kinase domain (Fig. 1.1).

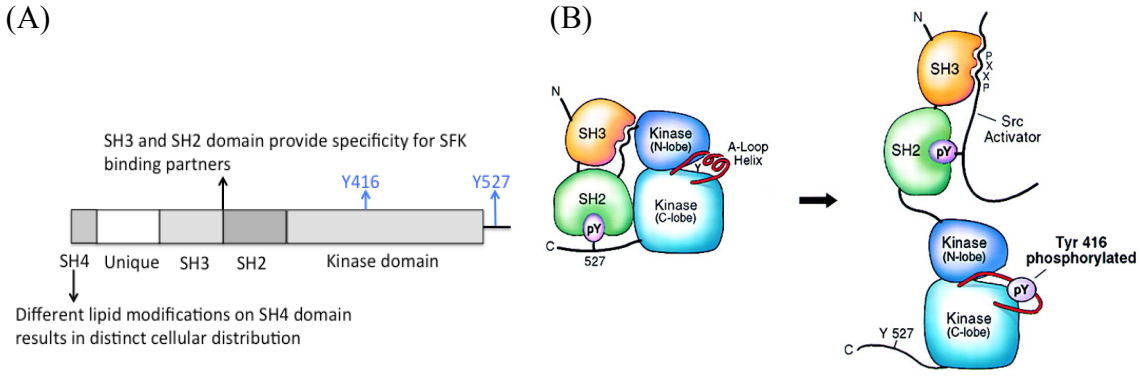

Figure 1.1. Structure and mechanistic regulation of Src.
(A) Domain organization of SFKs. SFKs share a similar domain arrangement. (B) A model of Src activation. Left, the inactive conformation of Src is stabilized by intramolecular interactions among the kinase domain, SH3-SH2 domains, and the C terminal tail. Right, the active conformation is initiated by dephosphorylation of Tyr527 and reorganization of the A-loop, thereby leading to the phosphorylation of Tyr416. (Figure 1.1B was adopted from Xu *et al.*, *Mol. Cell.* 1999 (47)).

The SH4 domain contains lipid modification sites, which cause membrane association and affect kinase distribution (48). The variability of lipid modifications among SFKs results in distinct cellular distributions, suggesting roles for functional specificity. The Unique domain is composed of a distinctive sequence for each SFK and its function remains largely unclear. A recent study by Perez *et al.* proposed that the Unique domain regulates membrane association of Src, in addition to its SH4 domain (49). The SH3 and SH2 domains play two important roles in kinase regulation; they stabilize the inactive conformation of Src via

intermolecular interactions and also provide binding specificity for its cellular substrates (50-53). Crystallographic studies have shown that the phosphorylated C-terminal tyrosine (Y527) associates with the SH2 domain, and the SH3 domain binds to the kinase domain, resulting in a closed conformation of Src (Fig. 1.1B). Dephosphorylation of Tyr527 releases the autoinhibited structure of Src and stimulates its catalytic activity by autophosphorylation of tyrosine 416 (Y416). The kinase domain of Src is composed of an N-terminal lobe and a C-terminal lobe. The smaller N-lobe is mostly comprised of antiparallel β-sheets and primarily involved in anchoring and orienting ATP. The larger C-lobe is composed of α-helical structure and mainly responsible for substrate binding. The cleft between the N-lobe and C-lobe, which serves as the ATP binding pocket, is important for catalytic activity (Fig. 1.2) (54). Intensive efforts have been made to understand the structural characteristics of ATP binding sites for regulating kinase activity. In summary, the stability of the glycine-rich loop (G-loop), orientation of the αC helix and the conformation of the activation loop (A-loop) are critical for regulating ATP binding and catalytic activity (55-57). To specifically regulate kinase activity for each Src family member, leaving other functional domains intact, we decided to manipulate the ATP binding pocket to gain absolute control of kinase activity for Src family kinases.

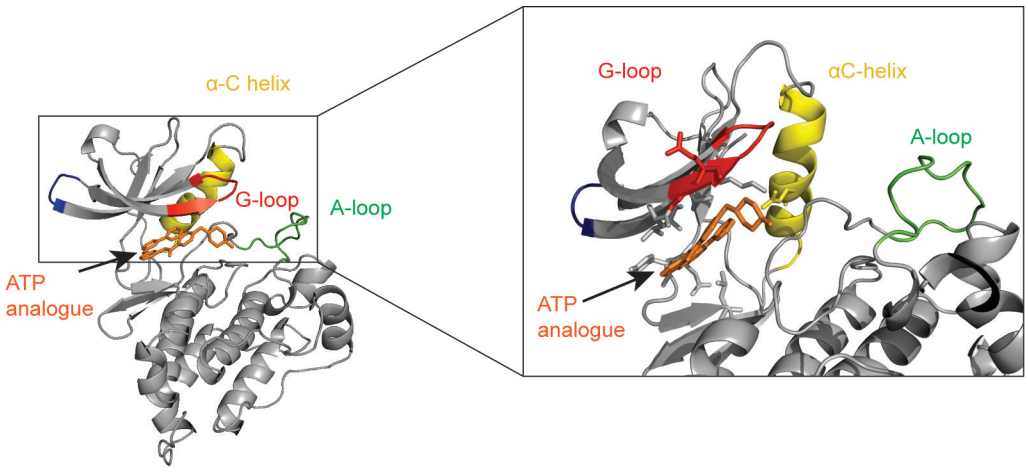

Figure 1.2. Structure of the Src catalytic domain.

Key structural elements are colored in red (G-loop), yellow (αC helix), and green (A-loop). The residues comprising the ATP binding pocket are shown as sticks (Zoom in, on the right). The ATP analog is shown in orange. (PDB: 1Y57).

CHAPTER TWO: A NEW TOOL FOR ACTIVATION OF SPECIFIC SRC FAMILY ISOFORMS AND ITS USE TO DEMONSTRATE SPECIFIC ROLES FOR ISOFORMS IN CELL MOTILITY

2.1 Overviews

The Src family kinases (SFKs) are composed of nine highly homologous members that participate in a diverse spectrum of signaling pathways. Similarities in their structure and regulation have made it difficult to separate the roles of each family member. To identify unique functions for individual SFKs, rapamycin-regulated (RapR) analogs of Src, Fyn, Yes, and Lyn were generated by insertion of an engineered FKBP domain into a conserved region of the kinases' catalytic domain. The catalytic activities of the analogs are greatly reduced and can only be restored by addition of rapamycin. The RapR analogs provide absolute control of specific Src family members and reveal the immediate cellular effect of individual SFK activation. The cellular morphodynamics and corresponding kinase translocations induced by specific SFK activation were characterized using new computational methods, revealing distinct roles for each isoform. Activation of Src and Fyn both initially generated cell spreading. However, only activation of Src induced polarized movement of the cell. We were able to convert the effects of Fyn activation to those of Src by mutating regions within Fyn important for lipid modification of the kinases. In addition, Src and this mutated version of Fyn translocate into adhesions and exhibit faster adhesion turnover, which facilitates cell

motility. Mutagenesis studies showed these distinct functions were mediated by specific acylation motifs leading to differential subcellular localization and translocation upon activation, and differential interaction with adhesion complexes.

2.2 Introduction

Src family kinases have been implicated as key regulators of ligand-induced cellular responses including proliferation, survival, adhesion, and migration (23, 54, 58). Fibroblasts from mice lacking the Src kinases Src, Fyn, and Yes (SYF cells) show impaired migration ability and reduced fibronectin-induced tyrosine phosphorylation of focal adhesion proteins (59). One of the major functions of SFKs is to control cell migration in normal cells; when kinases are dysregulated it leads to metastasis. Morphological changes induced by Src have been intensively studied in the past (60, 61). It is well accepted that activation of SFKs results in cytoskeleton rearrangement and causes cell transformation (62). However, whether individual SFKs contribute to distinct roles in cell motility has not been elucidated due to the lack of specific activators or inhibitors. The tools developed in this study provide specific temporal control of kinase activity and allow us to reveal the direct cellular responses of activating specific SFKs without cell compensation. The innovation can be summarized as follows:

1) Specificity – The rapamycin approach only activates engineered proteins containing the FKBP insertion. Compared with using a growth factor to induce SFK activation, this method allows investigation of the direct effects caused by targeted activation of a specific SFK.

2) Temporal activation – Rather than using a constitutively active form of an SFK to study cellular function, the RapR-SFKs allow us to observe the transient change from inactive to active. Moreover, rapamycin, which is cell permeable and allows for rapid activation of the kinase, is amenable to studies using a mouse model. This tool can avoid the compensation caused by overnight expression, wherein cells may initiate other mechanisms to overcome the gain/loss of a gene.
3) Minimum perturbation of cellular biology – Without expressing the active forms of kinases, the RapR-SFK strategy provides a way to regulate specific SFKs with minimum perturbation. Expression of active kinases at high levels causes hyperphosphorylation even before experiments can be started. In contrast to the active form of the kinase, the RapR-SFK is in an inactive state in the absence of rapamycin. There are no significant differences in cell morphology among cells expressing individual RapR-SFKs in our study. In addition, the distribution of fluorescent protein tagged RapR-SFKs is consistent with the distribution of endogenous SFKs.
4) Ability to control the activation of engineered RapR-SFKs – The rapamycin strategy allosterically controls only the catalytic domain of the kinase without affecting other domains, which interact with downstream effectors. Therefore, we can use RapR-kinase chimeras to study the specificity and functional contribution of individual SFK domains.

The high specificity and tight temporal control of kinase activity provided by the tools developed in this study allow us to activate individual SFKs and reveal their direct

cellular responses for the first time. Applying this strategy, we show the difference in cell responses upon Fyn and Src activation using RapR-Fyn and RapR-Src. Additionally, we use the modified RapR-kinases to examine the specific roles of functional domains in Fyn and Src. Ultimately, using these tools, we find that the cellular localization of kinases is critical to decide the cellular responses induced by kinase activation.

2.3 Results and Discussion

Generating specific regulators for Fyn, Yes, and Lyn

To dissect the unique roles of the SFK isoforms, we engineered regulatable Src, Fyn, Yes, and LynA kinase using the RapR strategy (63). The truncated form of insertable FKBP12 (iFKBP) was inserted into a conserved region in the catalytic domain, resulting in inhibition of kinase activity. The activity of the engineered kinase was rescued by rapamycin treatment in the presence of the FKBP12-rapamycin binding domain (FRB) (Fig. 2.1A). The iFKBP was inserted into a defined loop (named the insertion loop), which is directly linked to the glycine-rich loop (G-loop) via a β-strand. The G-loop controls nucleotide affinity and phosphoryl group transfer, which is important for catalytic activity (64-66). The structural flexibility of the G-loop has been reported to have significant effects on catalytic activity. The increased fluctuation of the G-loop upon insertion of iFKBP changed the binding and orientation of ATP, thereby greatly reducing catalytic activity (67). Addition of rapamycin rigidified the G loop, restoring catalytic activity (63). Based on the structural similarities of the catalytic domains in most tyrosine kinases, we were able to identify the G-loop and

insertion loop (Fig. 2.1B) for the other kinases, and applied this strategy to generate rapamycin-regulated analog of the SFK members Fyn, Yes, and LynA.

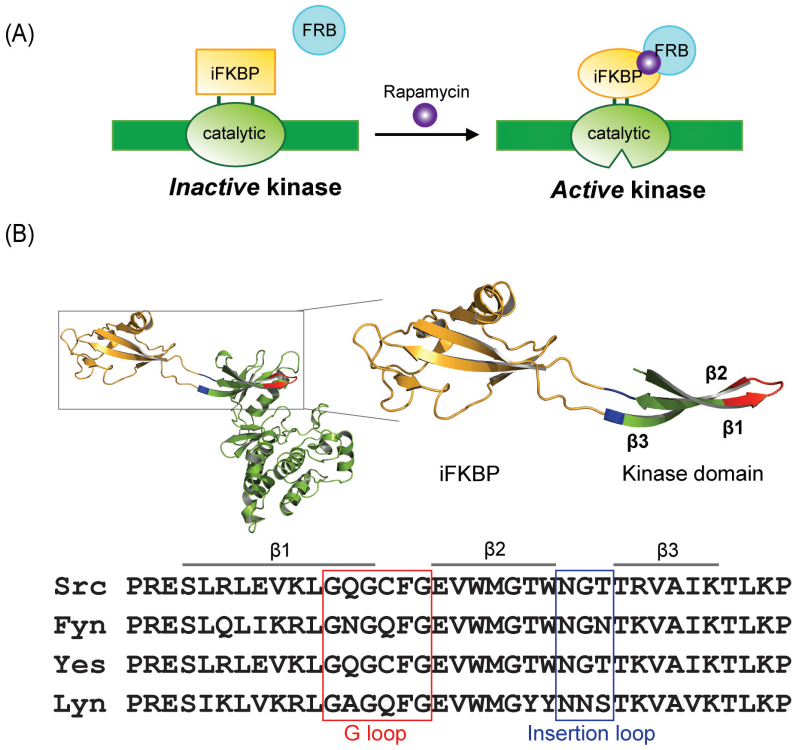

Figure 2.1. Design of RapR-kinases.

(A) Schematic representation of the approach used to regulate the catalytic activity of the kinases. Insertion of iFKBP into the catalytic domain of the kinase generated an inactive kinase. The catalytic activity can be recovered by adding rapamycin. (B) Identification of the insertion site for iFKBP. Sequence alignment of Src, Yes, Fyn, and LynA. The insertion loop (blue) is linked to the G-loop (red) directly through a β-sheet.

To optimize the regulation of kinase activity by iFKBP insertion, we tested various linkers connecting iFKBP to the catalytic domain of Fyn (Fig. 2.2A). A constitutively active mutation (CA) was included in the engineered kinases to release the autoinhibited structures. Activation of each RapR-kinase by rapamycin was demonstrated using *in vitro* kinase assays (described in detail in Materials and Methods). The kinase/FRB complex only formed in the

presence of rapamycin in cells expressing engineered kinases. The engineered Fyn, which used a longer linker (3GSPG/GPG) to insert iFKBP, showed less effect on restoring the catalytic activity upon rapamycin treatment. This suggests that the longer linker could not propagate the conformational changes of iFKBP to the G-loop, and thereby inefficiently restored the catalytic activity. Thus, to generate RapR-Yes and RapR-LynA, we used the short linker (GPG/GPG) to insert iFKBP into the catalytic domain. For RapR-Yes and RapR-LynA, iFKBP was inserted into the insertion loop by replacing the glycine and asparagine residues, respectively. All engineered kinases were able to regain catalytic activity upon treatment with rapamycin (Fig. 2.2B). The catalytically dead mutation (KD, mutation D388R) was included to generate the RapR-kinase-KD as a negative control. The RapR-kinase-KD was inactive regardless of the presence of rapamycin, suggesting that rapamycin-induced Paxillin phosphorylation was caused by the catalytic activity of kinase.

(A)

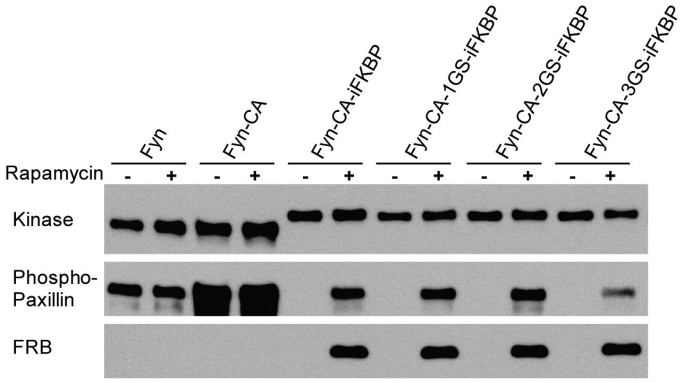

Fyn -TWNGNTKV
Fyn-CA -TWNGNTKV
Fyn-CA-iFKBP -TWNG-**PG**-iFKBP-**GPG**-NKTV
Fyn-CA-1GS-iFKBP -TWNG-**GSPG**-iFKBP-**GPG**-NKTV
Fyn-CA-2GS-iFKBP -TWNG-**GSGSPG**-iFKBP-**GPG**-NKTV
Fyn-CA-3GS-iFKBP -TWNG-**GSGSGSPG**-iFKBP-**GPG**-NKTV

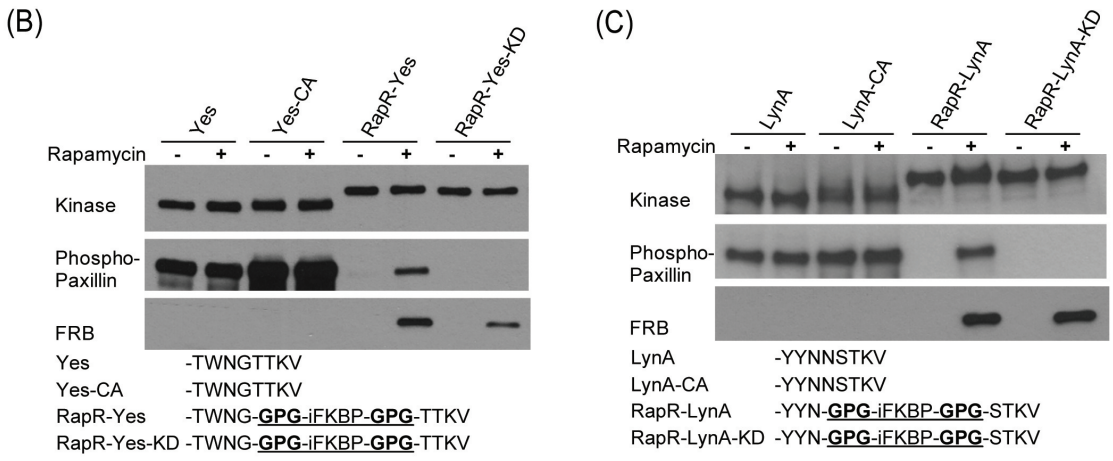

Figure 2.2. Biochemical characterization of RapR-kinases.

(A) Various linkers were used to insert iFKBP into the insertion loop of Fyn kinase, and the activity of the engineered kinases can only be rescued by rapamycin treatment. The kinase assay was performed using purified Paxillin as a substrate, and phosphorylation reactions were observed using an anti-phospho-Paxillin antibody. (B) The GPG linker was used to insert the iFKBP fragment into Yes and LynA to generate RapR-Yes and RapR-LynA. The regulation of kinase activity by rapamycin was determined using an anti-phospho-Paxillin antibody.

The RapR-kinases provide absolute control of each SFK member and allow us to reveal the direct effects of activating individual Src family members for the first time.

Activating individual SFKs generates distinct morphological changes

Morphological transformation due to overexpression of v-Src or active c-Src has been intensively studied in the past (60, 61). The transforming ability of other SFK members were also examined in Oneyama's study. All SFKs have been shown to induce cell transformation when expressed in fibroblasts lacking a negative Src regulator (Csk) (62). However, whether

individual SFKs contribute to distinct roles in morphological changes has not been elucidated. To examine whether individual SFKs stimulate different cellular responses, each SFK was activated specifically and independently using the RapR-kinase strategy. Individual RapR-SFKs were co-expressed with FRB in COS-7 cells and activated by rapamycin treatment. Due to the observation that all SFKs have transformation potential, it was surprising that the activation of a specific SFK induced distinct morphological changes in the early stage of activation (Fig. 2.3). Activation of Fyn generated uniform spreading, while activation of Src initiated polarized movement. LynA, which is mainly expressed in hematopoietic cells, induced a completely different phenotype. Activation of Lyn induced long membrane projections that did not attach to the matrix. Only 10% of cells expressing LynA generated this distinct behavior upon activation, due to the low expression efficiency. Activation of Yes induced a phenotype in between those seen with Src and Fyn activation, wherein cells were spread in the early stage and later generated polarized movement in a delayed manner.

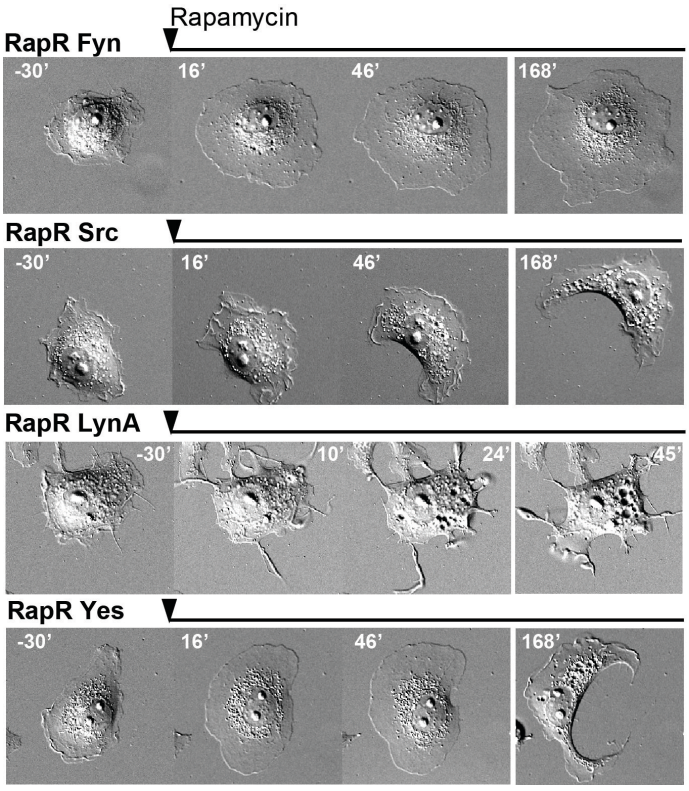

Figure 2.3. Distinct morphological changes result from activating specific SFKs using rapamycin.

Time-lapse imaging of COS-7 cells expressing specific RapR-kinases was used to study the effects of specific SFK activation. Cell responses were monitored 30 minutes before activation and rapamycin was added at time zero, to stimulate kinase activity. Representative images from cells expressing each RapR kinase demonstrate the distinct cellular responses induced by kinase activation (n>55 cells).

Quantification of morphological changes using a new computational method

In the absence of specific activators for individual SFKs, research was conducted by overexpressing the active forms of specific SFKs to study their functions. Expressing the active forms of SFKs all resulted in the same transformed phenotype, without any temporal

information. Differences in cellular responses in the early stage of SFK activation were not found in previous studies. Using the RapR strategy, we were able to reveal different responses induced by individual SFK activation for the first time. To objectively evaluate the effects of RapR kinases on cell morphology, we collaborated with Dr. Denis Tsygankov and Dr. Tim Elston to develop a new computational method to automatically characterize cell behaviors over time. This approach defines a morphological signature for each consecutive time step using two simple parameters created by the method. The two parameters, growth rate and polarization, were generated based on the motions of the cell boundary. Cell boundary motion was characterized with respect to the boundary position at the previous time step. The relative motions of the corresponding boundary points were recorded as boundary displacements, containing both direction and magnitude information. The rate of cell area changes (growth rate, R_{cr}) can be determined by the sum of these displacements. By mapping the displacements onto a circle, we introduced a generic measurement for cell polarity (polarization, P_{cr}) between consecutive time points (Fig. 2.4).

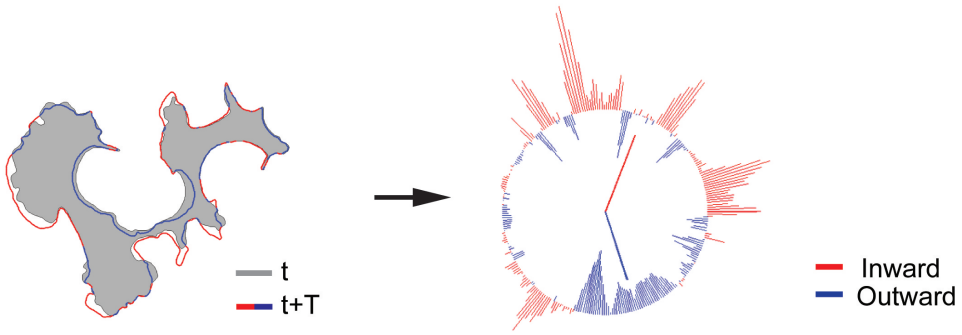

Figure 2.4. The rationale of the quantitative method used to characterize cell morphological changes.

Cell boundary motions are obtained from consecutive time points. The red and blue lines represent the relative motion between the two time points. Displacements are generated for each boundary point to represent its inward/outward motion. The sum of the direction and

magnitude of displacements at this time step are shown as red/blue lines in the middle of the circle.

A parameter space was constructed using R_{cr} and P_{cr} measurements. The dynamics of cell motion were represented as a trajectory, allowing the complicated dynamics of a cell to be recorded in a single parameter space. By setting up the thresholds for these two parameters (R_{cr} and P_{cr}), the parameter space was divided into six regions with each region representing a defined cell behavior: unchanged, uniform spread, polarized spread, polarized movement, polarized shrinkage and uniform shrinkage (Fig. 2.5A). Figure 2.5B shows a representative example using this method to characterize morphological changes over time. The upper panel shows cell motions for all time steps recorded as a trajectory in the parameter space. The cell behavior for each time step was defined according to the location of the measurements within the parameter space. The lower panel displays a graphic representation of cell shape changes at consecutive time steps from a real experiment. The defined cell behaviors correspond to the cell shape changes observed from the experiment (a→b: Uniform spread, b→c: Polarized movement, c→d: Polarized shrinkage, d→e: Uniform spread). This quantitative method allowed us to define morphological signatures for each time step and to compress all the information into a single parameter space.

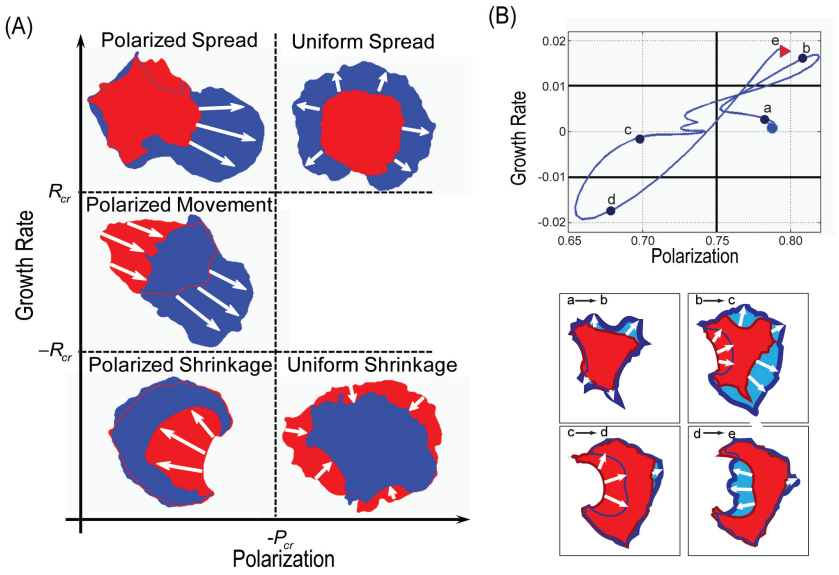

Figure 2.5. Illustrations of the method used to characterize cell morphological changes over time.

(A) Parameter space was defined using two measurements generated from relative cell boundary motion in consecutive images. Different regions of this parameter space each represent a defined cell behavior. The images from previous time points are shown in red and the sequential images are shown in blue. The directions of cell boundary movement are indicated using arrows. (B) Dynamic cell motions are represented as a trajectory in the parameter space. The lower panel shows the shape changes between the previous time point (red) and the next time point (blue).

Src and Fyn induce distinct morphological changes upon activation

To address concerns about heterogeneity from experiments using single cell assays, we processed the images from over 55 cells for each kinase tested. For every time step, we determined a defined cell behavior using the cell's measurements in the parameter space. Each behavior generated a value, indicating how many cells underwent a particular behavior at a given time. The statistical results were displayed in three types of graphs: character plot,

scatter plot, and percentage plot. Each display served different purposes for data interpretation.

The character plot represents the morphological signature for each RapR-kinase. In this plot, the z value (phenotype prevalence) is the moving average (5-frames window) of cell counts doing a particular behavior at a given time point. The character plot in figure 2.6 indicates that both activation of Fyn and Src initially induced a profound spreading phenotype but only Src followed with polarized movement in the later stages of activation.

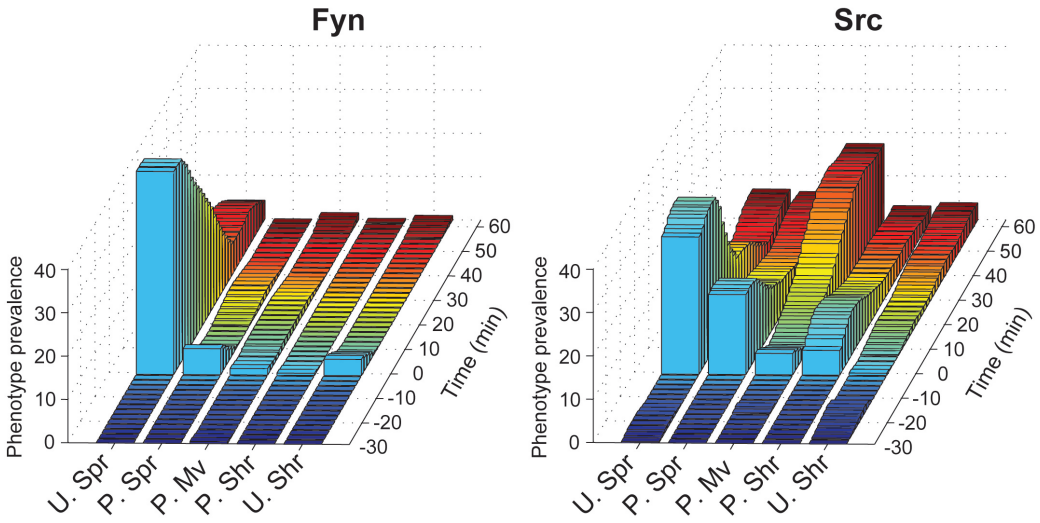

Figure 2.6. Distinct morphological changes are induced by activating Src and Fyn. The morphological signature of each RapR-kinase can be revealed using the quantitative method developed in this study. Morphological changes induced by kinase activation were quantified as described in Figure 2.5 over more than 55 cells expressing RapR-Fyn or RapR-Src. The z-axis value represents the prevalence of the defined behavior for each time step. U. Spr: uniform spread; P. Spr: polarized spread; P. Mv: polarized movement; P. Shr: polarized shrinkage and U. Shr: uniform shrinkage.

The scatter plot provides an unbiased way to display cell behaviors from the whole cell population. Each point in the parameter space represents one single cell at a given time

point. The distribution of points in the parameter space gives an overview of the overall behaviors for all the cells in a 30-min period of time (Fig. 2.7). The red lines indicate the threshold values that were used to separate the types of cell motion. During the period of time without rapamycin treatment (-30 to 0 min), both Fyn and Src were restricted to the "unchanged state" space (the middle space on the right) and displayed no significant morphological changes before kinase activation. During the early stage of kinase activation by rapamycin (0 to 30 min), the distribution of Fyn cells in the parameter space shifted toward the "uniform spreading" space. Activation of Fyn induced transient changes in cell morphology within the first thirty minutes. The morphology of Fyn cells did not change much in the following time period (30 to 60 min), and the distribution of measurements returned to the "unchanged state" space (Fig. 2.7A). On the other hand, in the early stage of Src activation (Fig. 2.7B, 0 to 30 min), cells showed four different behaviors besides uniform shrinkage. Src cells exhibited mostly polarized movement in the later stage of activation, while very few Fyn cells underwent polarized movement during the same stage (30 to 60 min).

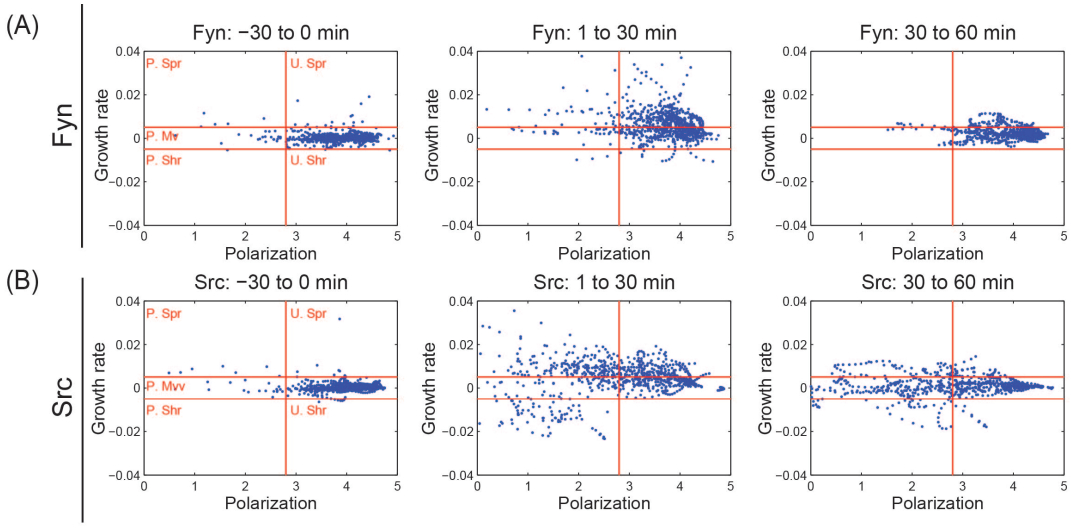

Figure 2.7. Scatter plots reveal morphological changes among all the cells over time. Each dot (blue) represents a single cell at a given time step determined by two values (growth rate and polarization) obtained from relative cell motions. Morphological changes induced by kinase activation were quantified over more than 55 cells expressing RapR-Fyn or RapR-Src. The red lines indicate the thresholds constructing the parameter space. In the parameter space, the middle region on the right represents the unchanged state. Other regions are labeled as followed: U. Spr: uniform spread; P. Spr: polarized spread; P. Mv: polarized movement; P. Shr: polarized shrinkage and U. Shr: uniform shrinkage.

The third display, the percentage plot, was used to describe whether the majority of cells are exhibiting a certain behavior at a precise time step. The black line (None) in the upper part of the graph indicates the percentage of cells considered non-responsive in this analysis, with the measurements located in the unchanged state region of the parameter space. In the lower part of the graph, each colored line represents a particular behavior defined using this computational method. Rapamycin was added at time zero to activate Fyn or Src, specifically. Before kinase activation, both cells expressing RapR-Src and RapR-Fyn were considered non-responsive. The majority of cells expressing RapR-Fyn induced uniform spreading immediately after activation and up to 60 % of cells responded to the rapamycin treatment. Cells expressing Src exhibited uniform spread, polarized spread, and polarized shrinkage to different degrees. The polarized movement occurred after 35 minutes of activation and lasted for the entire course of experiment (Fig. 2.8).

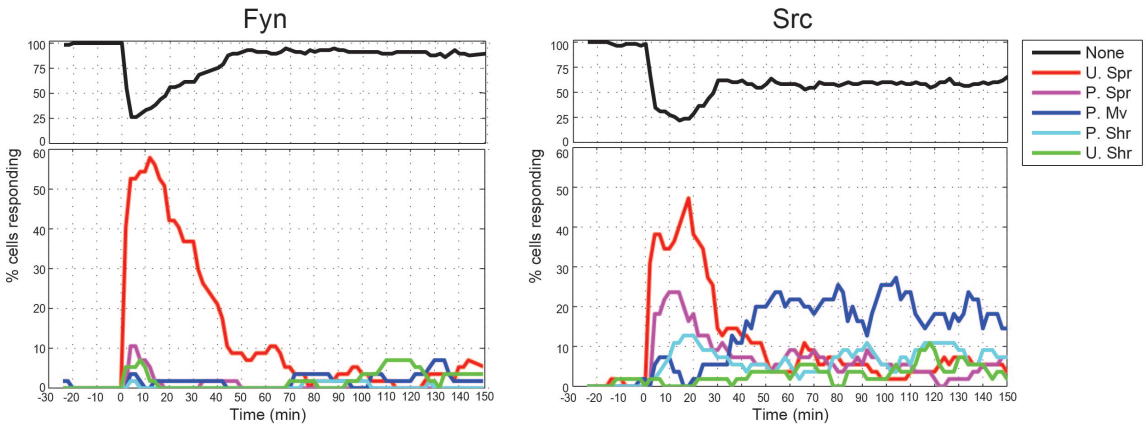

Figure 2.8. The percentage plot reveals the population of cells exhibiting a particular behavior over time.

The graph is separated into two parts. The upper part of the graph shows the percentage of cells considered non-responsive and the lower part of the graph depicts the percentage of cells responding to each defined behavior. Morphological changes induced by kinase activation were quantified as described in Figure 2.5 over more than 55 cells expressing RapR-Fyn or RapR-Src. U. Spr: uniform spread; P. Spr: polarized spread; P. Mv: polarized movement; P. Shr: polarized shrinkage and U. Shr: uniform shrinkage.

Src, Fyn, and Yes are ubiquitously expressed in most cell types. Using the RapR strategy, we were able to reveal the distinct morphological changes during the early stage of activation for each isoform. The computational analysis suggested that Src and Fyn induce distinct morphological changes, while Yes exhibits a morphological signature in between Src and Fyn (Figure 2.9). In the next section, I will focus on the potential mechanisms causing the differences between Src and Fyn activation.

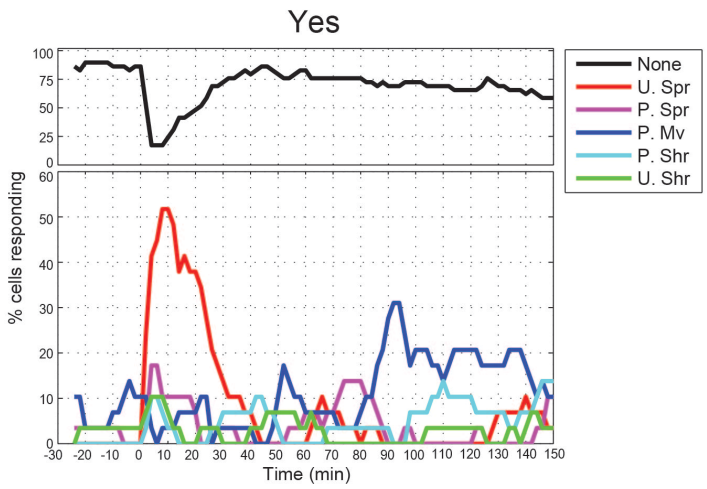

Figure 2.9. Activation of Yes-induced morphological changes with features of both Src and Fyn.

The graph is separated into two parts. The upper part of the graph shows the percentage of cells considered non-responsive, and the lower part of the graph depicts the percentage of cells responding to each defined behavior. Morphological changes induced by kinase activation were quantified as described in Figure 2.5 over more than 55 cells expressing RapR-Yes. U. Spr: uniform spread; P. Spr: polarized spread; P. Mv: polarized movement; P. Shr: polarized shrinkage and U. Shr: uniform shrinkage.

To investigate whether a particular phenotype was dependent on the expression levels of the RapR-kinase in the cell, we separated the cells into two groups based on the protein levels of the expressed RapR-kinase and analyzed their morphological signatures. Neither Src nor Fyn showed particular morphological signatures biased towards a specific expression level (Fig.2.10).

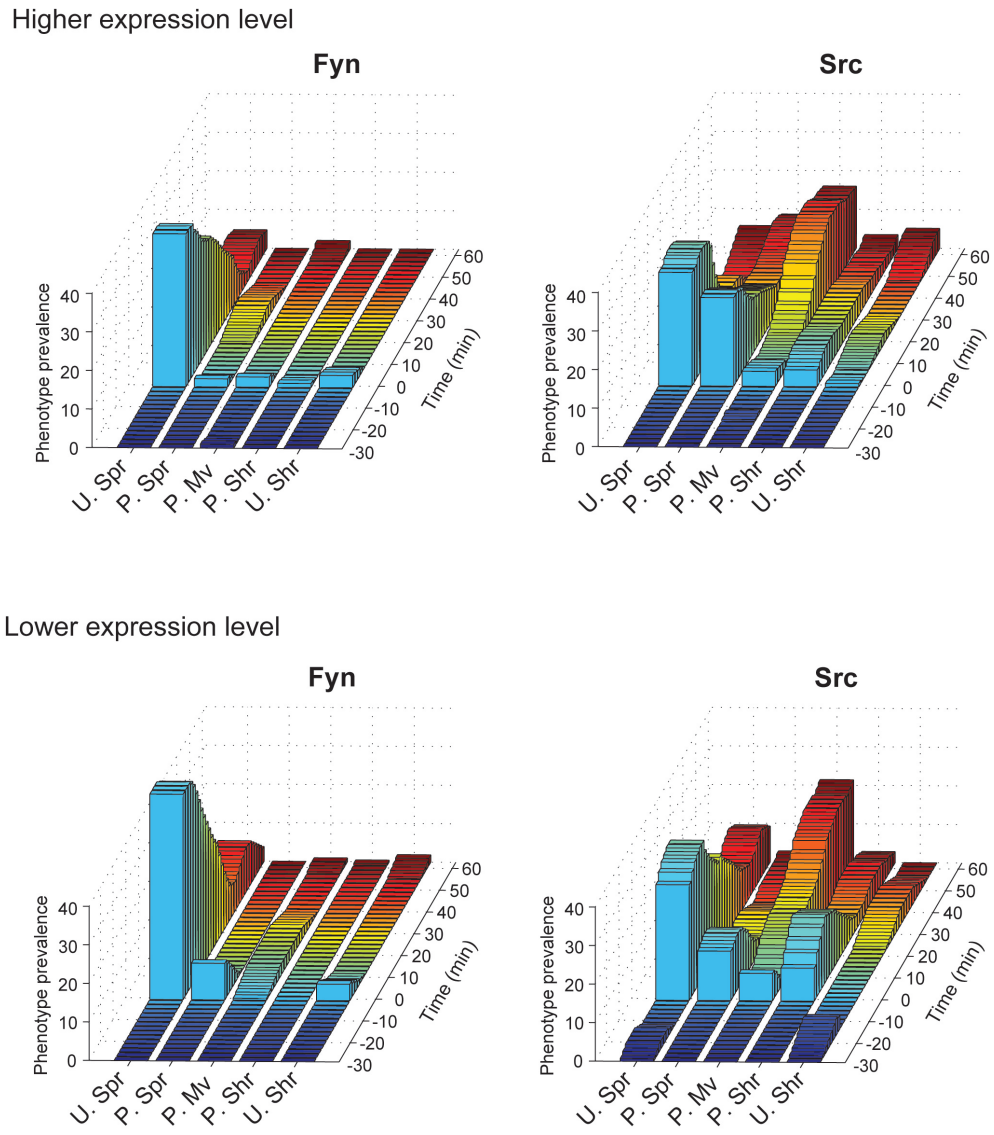

Figure 2.10. The morphological signatures of cells induced by Src and Fyn activation are not dependent on expression levels of RapR-kinases.

Cells were binned into high and low expressers and the behavior of each population was quantified on an individual cell basis as described in Figure 2.5 (n>55 cells). U. Spr: uniform spread; P. Spr: polarized spread; P. Mv: polarized movement; P. Shr: polarized shrinkage and U. Shr: uniform shrinkage.

The morphological changes induced by SFK activation depend on the activities of their cellular substrates, which are determined by their phosphorylation states. To confirm that the cell behaviors induced by RapR-kinases are not an artifact from the engineered proteins, we compared the phosphotyrosine protein profiles for cells expressing active SFKs versus RapR-SFKs upon treatment with rapamycin. The phosphorylation profiles of cells expressing the active kinases and RapR-SFKs were similar. Auto-phosphorylation of the expressed proteins (labeled as SFK and RapR-SFK) was found in both samples containing the active forms of the expressed kinases and RapR-SFKs. Cells expressing kinases containing the inactive mutation (kinase dead, KD) showed a lesser degree of phosphorylation on the total substrate (Fig. 2.11).

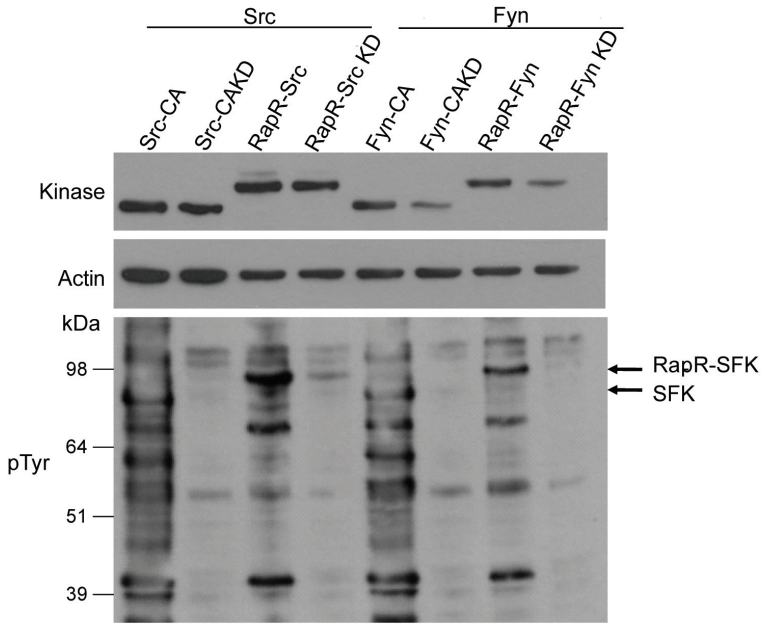

Figure 2.11. Comparison of the phosphotyrosine protein profiles of cells expressing active SFKs and RapR-SFKs.

The phosphorylation levels of total proteins from cells expressing fluorescent protein tagged kinases were analyzed by immunoblotting using an anti-pTyr antibody. (SFK, M.W.=87 kDa; RapR-SFK, M.W.=97 kDa) Protein levels of fluorescently tagged kinases were detected

using an anti-GFP antibody. Equal protein loading was determined using an anti-β-actin antibody.

Exchanging the SH3-SH2 domains of Fyn and Src does not affect the morphological signatures induced by kinase activation

To understand the mechanisms underlying the distinct cell responses caused by Src and Fyn activation, we examined the roles of different functional domains in changing cell morphology. One hypothesis is that the distinct responses induced by Fyn and Src are due to their interactions with different downstream effectors. The two conserved domains of SFKs, Src homology 3 and 2 domains (SH3 and SH2 domains), mediate intramolecular and intermolecular binding interactions, regulating the catalytic activity of kinases and the protein-protein interactions between kinases and substrates (68, 69). The SH3 domain recognizes proline-rich sequences to direct specific binding interactions, while the SH2 domain selectively binds to the substrate's phosphotyrosine moiety (70, 71). Distinct ligand preference via SH3-SH2 domains between SFK homologues has been demonstrated in previous studies (70, 72-74). To address whether the different binding partners are critical for distinct morphological changes, the SH3-SH2 domains were exchanged between Fyn and Src to generate Fyn/Src chimeras (named Fyn (SrcSH32) and Src (FynSH32)), shown in figure 2.12A. Surprisingly, changing the SH3-SH2 domains did not alter cellular responses when the chimeric kinases were activated. The cellular distributions of these chimeras were similar to those of their corresponding wild-type kinases. The majority of Fyn (SrcSH32) and Fyn were membrane bound, while Src (FynSH32) and Src were accumulated at the perinuclear space before activation (Fig. 2.12B). Activation of Fyn (SrcSH32) induced only uniform

spreading, similar to wild-type Fyn. Activation of Src (FynSH32) generated polarized movement in later stages of kinase activation, similar to that of Src but in a smaller population of cells (Fig. 2.12C).

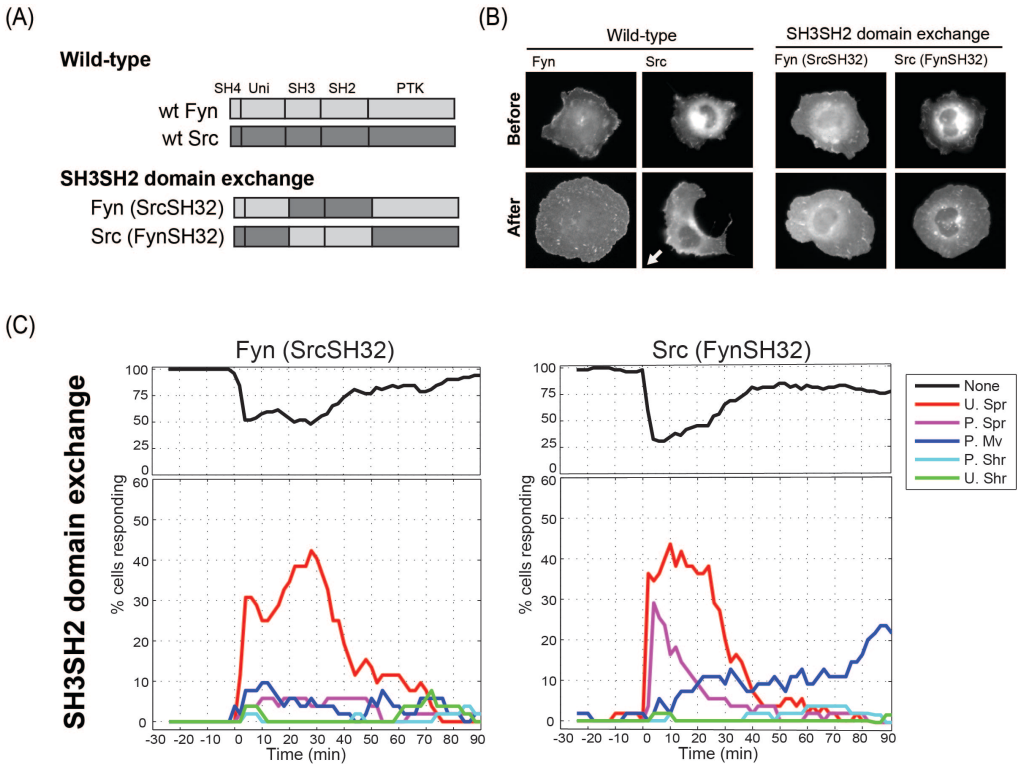

Figure 2.12. Exchange of the SH3-SH2 domains in Fyn and Src neither change the cellular distribution of the kinases nor affect the cell behavior generated by kinase activation.

(A) Illustration of the constructs used in the effector binding domain study. (B) Representative images for cells expressing chimeric kinases. (C) Percentage of cells responding for each behavior over time. Morphological changes induced by kinase activation were quantified as described in Figure 2.5 over more than 55 cells expressing chimeric kinases. U. Spr: uniform spread; P. Spr: polarized spread; P. Mv: polarized movement; P. Shr: polarized shrinkage and U. Shr: uniform shrinkage.

Src and Fyn exhibit different cellular translocation patterns upon activation

In addition to revealing the immediate responses of specific kinase activation, the RapR strategy also provides a way to monitor kinase translocation during the activation process. Although exchanging the effector-binding domains of Fyn and Src did not alter cellular response, we did notice that wild-type Fyn and Src exhibited different cellular distributions and translocation patterns during activation. To quantify the redistribution of the kinases, the intensity of the kinases within the perinuclear region and outside of the perinuclear region were used to measure kinase translocation. The two regions, the perinuclear ring and outside of the perinuclear ring, were automatically identified through a computational program based on the positions of the nucleus and the cell edge. The intensity ratio was measured using different perinuclear ring widths, and a defined width of 30 pixels was used in this method (Fig. 2.13A). The translocation of the kinases was quantified and is displayed in figure 2.13B. Fyn (black) and Fyn (SrcSH32) (pink) are represented as a flat line, indicating there was no change in kinase distribution before and after activation. The Src (red) and Src (FynSH32) (brown) exhibited a higher value before activation as compared to Fyn, suggesting Src has strong perinuclear accumulation. The decreasing value of the intensity ratio over time indicates that Src and Src (FynSH32) diffuse out from the perinuclear region after activation.

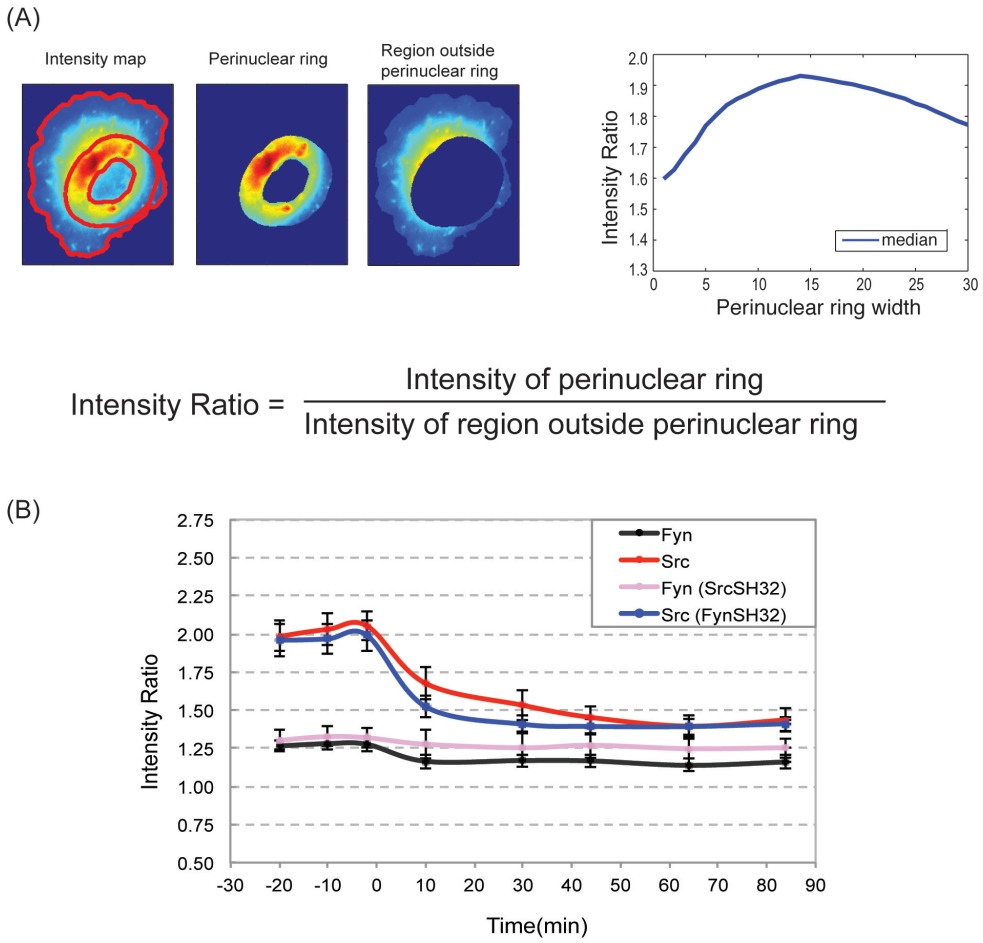

Figure 2.13. Quantification of kinase translocation during activation.

(A) Example of the defined regions used to generate the intensity ratio of the kinase. The intensity ratio was tested using different widths of the perinuclear ring. The ring width used in this study was 30 pixels (ten microns). (B) The intensity ratio for the constructs tested in this study represent the kinase translocation event over time. Intensity ratios were obtained from eight different time steps and kinases were activated at time zero. Error bars indicate 90% confidence intervals (n>55 cells).

Using confocal microscopy to confirm the cellular distribution of kinases observed from wide-field images

To confirm that the perinuclear spots observed from wide-field images of cells expressing fluorescently tagged RapR-Src were from the accumulation of expressed kinases in the perinuclear region, we examined kinase distribution along the Z-axis using confocal microscopy. The image of the middle section along the Z-axis is shown in figure 2.14A reveals the distribution of Fyn and Src. The intensity of pixels along the horizontal line was analyzed using line scanning (Fig. 2.14B). The results show that Src, but not Fyn, accumulates in the perinuclear region. Activation of Src resulted in kinase redistribution, and Src was released from the perinuclear region upon activation (Fig. 2.14 right panel).

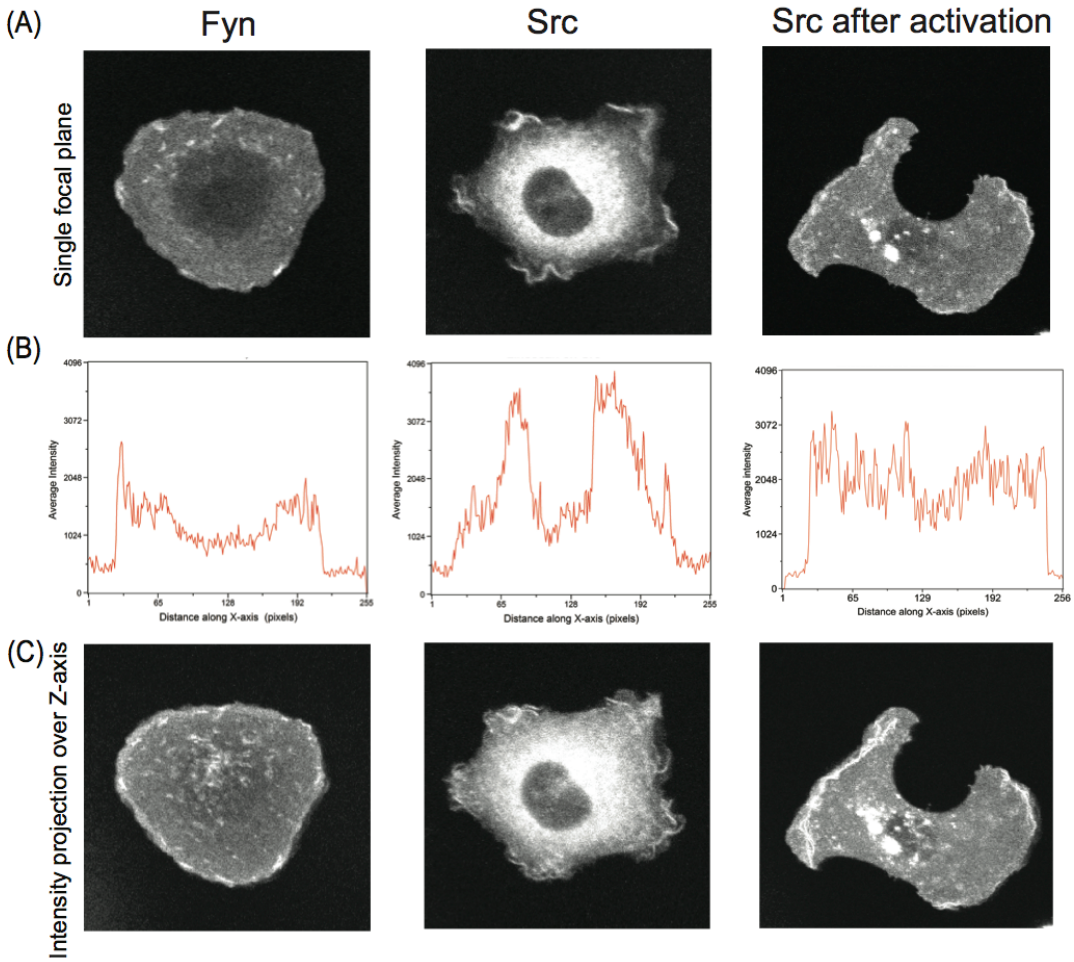

Figure 2.14. Cells expressing Src, but not Fyn, show kinase accumulation at the perinuclear region.

Fluorescently tagged Fyn and Src were imaged using confocal microscopy. (A) Single-focal plane images of cells expressing Fyn and Src before activation. (B) A representative horizontal line-scan from the image above. (C) Images of z-series projections.

Changing the cellular distribution of Fyn is sufficient to convert the morphological effects of Fyn activation into those of Src activation

Fatty acylation of SFKs, which occurs in their N-terminal SH4 domain, has been shown to influence their distribution and association with other cellular components (48). Both Src and Fyn are cotranslationally myristoylated on glycine at position 2, but only Fyn can be palmitoylated on cysteine at positions 3 and 6 (75). Fyn, with dual palmitoylation sites, is mostly associated with the plasma membrane (76, 77). Inactive Src, without palmitoylation sites, mainly accumulates in the perinuclear region, which is thought to be associated with endosomal and Golgi compartments (78, 79). The difference in acylation of Fyn and Src results in distinct cellular distributions, suggesting functional specificity. To determine whether changing the cellular distribution of SFKs is sufficient to alter the responses induced by activation, we altered the lipid modifications of Fyn and Src in their SH4 domains by introducing mutations (Fig. 2.15A). Both Cys3 and Cys6 of Fyn were substituted for serine to eliminate the addition of palmitoylated modifications (Fyn $Palm^-$). While wild-type Fyn is primarily localized to the plasma membrane, Fyn $Palm^-$ showed the same accumulation in Golgi compartments as wild-type Src (Fig. 2.15B). In addition to exhibiting the same cellular distribution before activation as Src, activation of Fyn $Palm^-$ also induced kinase translocation similar to wild-type Src (Fig. 2.15C). In the case of

palmitoylated Src (named Src Palm^{+}), changing the serine to cysteine at positions 3 and 6, only attenuated kinase accumulation in the perinuclear region. The kinase translocation analysis of Src Palm^{+} indicates that, by creating only two point mutations in the SH4 domain the kinase cannot be fully released from the perinuclear region.

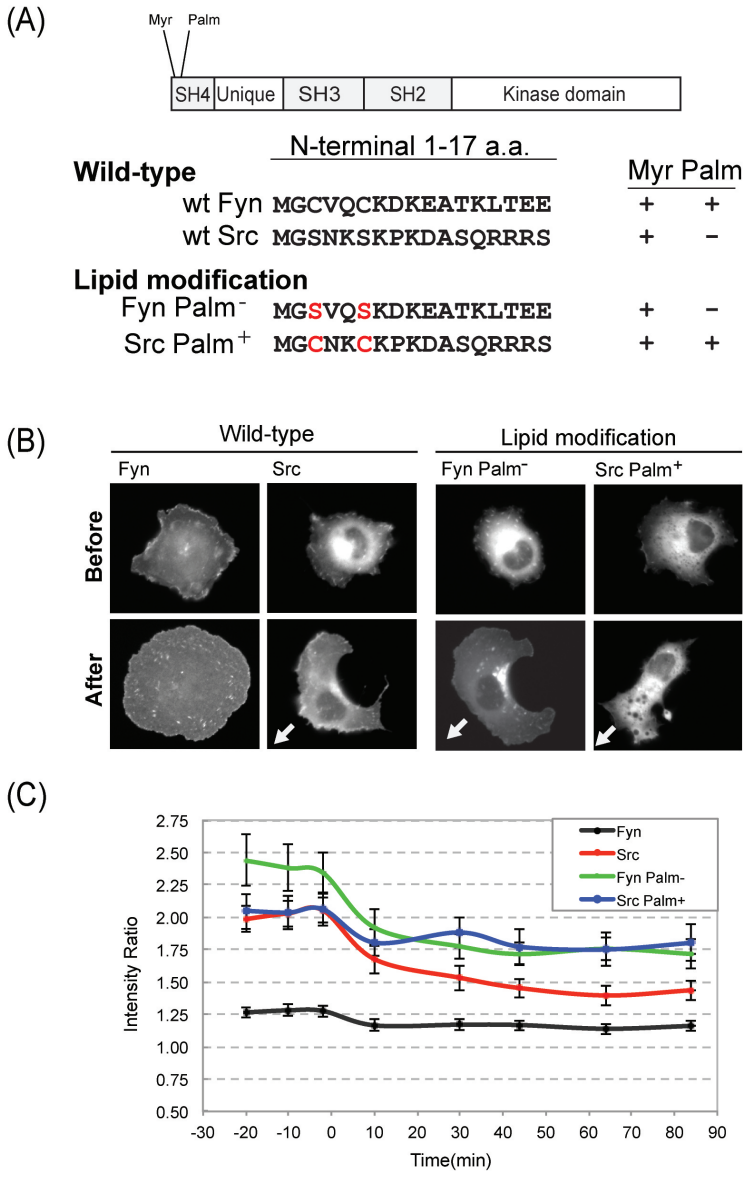

Figure 2.15. Changing the lipid modification sites of Src and Fyn results in different cellular distributions and translocation pattern of the kinases.

(A) Nomenclature for constructs of wild-type Src, Fyn, and their derivatives. The changes in amino acids are labeled in red. (B) Representative fluorescent images of cells expressing Src, Fyn, and their derivatives. The arrows (bottom panel) show the direction of migration. (C) The translocation of induced kinases was quantified by comparing kinase intensity in different regions of the cells at a given time point. Intensity ratios were obtained from eight different time steps and kinases were activated at time zero. Error bars indicate 90% confidence intervals (n>55 cells). Rapamycin was added at time zero to activate the engineered kinases.

To examine the correlation of kinase distributions and their cellular responses, the engineered kinases were activated by rapamycin. Altering the lipid modifications of Fyn (Fyn Palm$^-$) was sufficient to induce polarized movement. In contrast, Src Palm$^+$, which cannot be fully released from the perinuclear region after activation, generated a completely different phenotype than wild-type Fyn or Src.

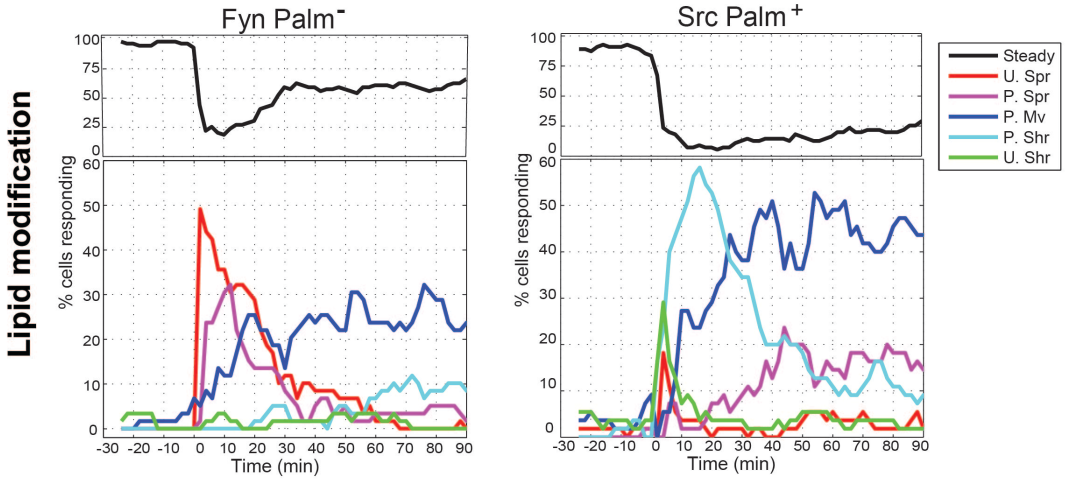

Figure 2.16. Cells expressing non-palmitoylated Fyn induced the same morphological changes as Src.

Graphs show the percentage of cells responding for each behavior over time. Rapamycin was added at time zero to activate the engineered kinases. The upper parts of the graphs show the

percentage of cells considered non-responsive (black). Kinases were activated at time zero. Error bars indicate 90% confidence intervals (n>55 cells).

In contrast to wild-type Src, Src Palm$^+$ induced profound cell shrinkage accompanied with non-directional movement (Fig. 2.17A). To distinguish the different modes of movement between Src and Src Palm$^+$, the mean-square-displacement (MSD) was calculated over time from cell centroid trajectories (Fig. 2.17B), and the directional persistence time was obtained by fitting these measurements to the persistence random walk equation. Persistence time characterizes the average time between significant changes in the direction of migration (80-82). Src Palm$^+$ showed a much lower persistence time (Fig. 2.17C). The quantitative results confirmed the observation that Src Palm$^+$ migrated in a non-directional mode, distinct from wild-type Src.

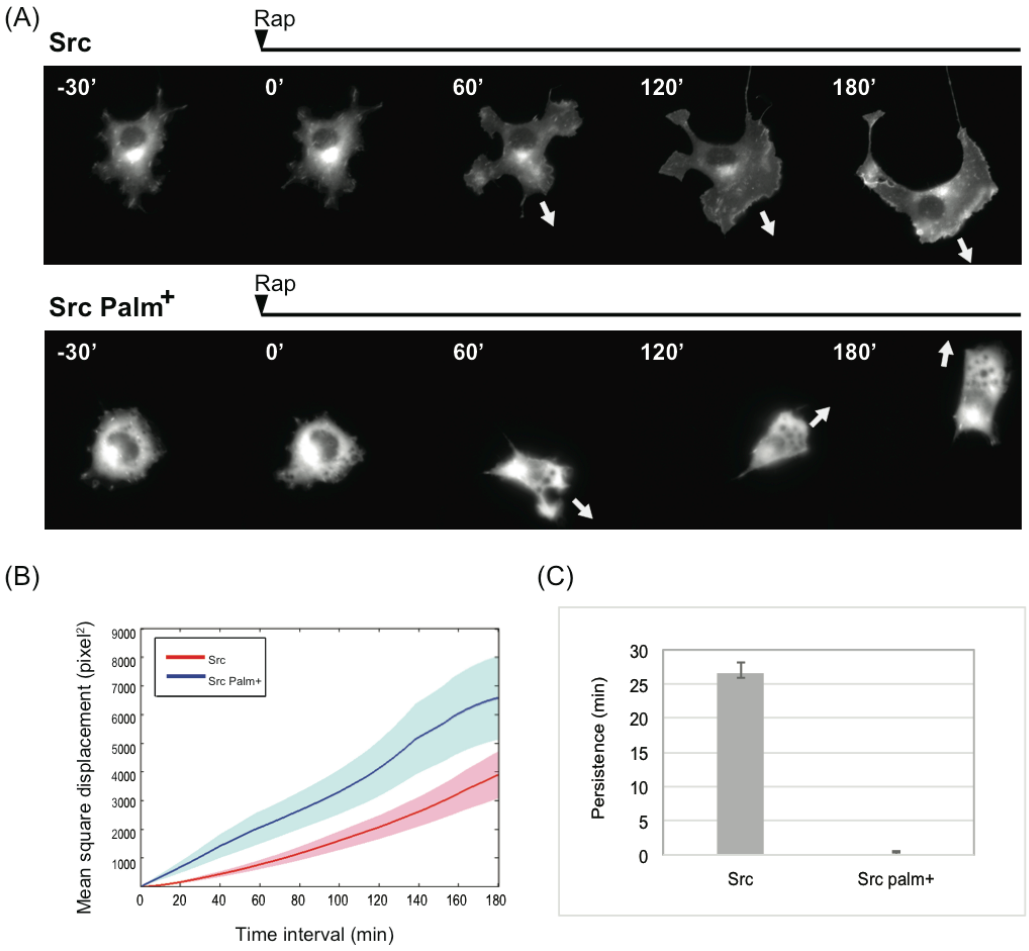

Figure 2.17. Activation of Src induced directed movement, while activation of Src Palm$^+$ resulted in non-directional movement.

(A) A representative example of a cell expressing Src and Src Palm$^+$. The arrows indicate the direction of movement. (B) The mean-square displacements were calculated by tracking the centroid movement. Shaded regions indicate standard error (n>55 cells). (C) The directional persistence obtained from a population of cells (n>55 cells) by fitting the resulting curve to a persistent random walk to compute an estimate for the persistence of centroid movement. Error bars, standard error of persistence time.

Replacing the SH4-Unique domain of Src with the SH4-Unique domain of Fyn alters the kinase distribution and cellular response of Src upon activation

Studies of Src membrane association show that mutation of Ser3 and Ser6 in Src display a mild incorporation of the palmitate analog as compared to a Fyn-Src chimera, which the entire SH4 domain of Src was replaced with the SH4 domain of Fyn (77). This result is consistent with the cellular distribution we observed in our Src $Palm^+$ mutant. In addition, Perez *et al.* proposed that the Unique domain of Src provides additional regulation of its interaction with lipid compartments (49). Therefore, in order to generate Src derivatives that can mimic the cellular distribution of Fyn, the SH4-Unique domain of Fyn was used to replace the SH4-Unique domain of Src (named Src (FynSH4U)) (Fig. 2.18A). Src (FynSH4U) displayed dramatically decreased perinuclear accumulation (Fig. 2.18B). Cells expressing Src (FynSH4U) showed a higher intensity ratio measurement as compared to Fyn, with a slight decrease after activation (Fig. 2.18C, orange line). This indicates that small amounts of kinase were still able to accumulate at the perinuclear region and undergo redistribution after activation. Activation of Src (FynSH4U) resulted in uniform spreading, with a duration of spreading behavior similar to that of Fyn. However, polarized movement still occurred after the uniform spreading, but was delayed compared to the polarized movement of cells expressing wild-type Src (Fig. 2.18D). The prolonged uniform spreading and delayed polarized movement may result from the small amount of kinase accumulation in the perinuclear region before activation.

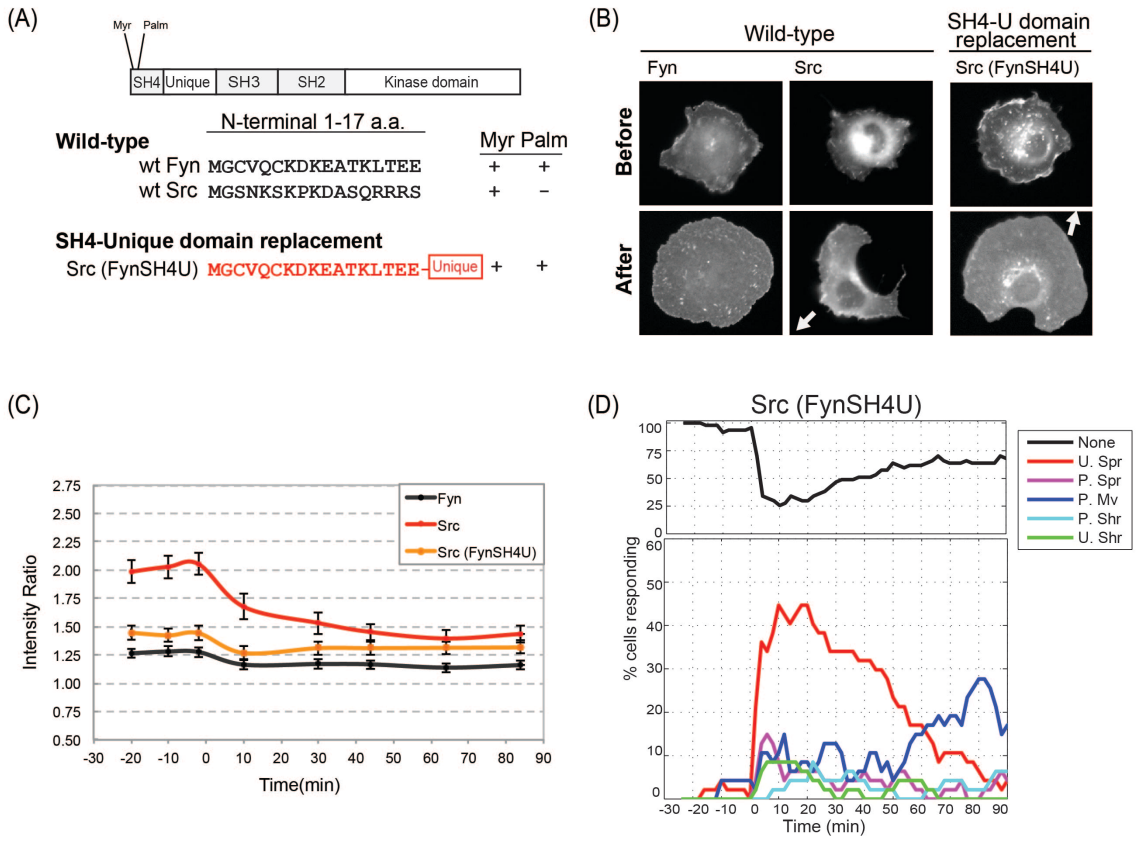

Figure 2.18. Replacing the SH4-Unique domain of Src with the SH4-Unique domain of Fyn induced prolonged uniform spreading behavior.

(A) Illustration of construct designs for wild-type Src, Fyn, and Src (FynSH4U). The changes in sequence and domains are labeled in red. (B) Representative fluorescent images of cells expressing Src, Fyn, and Src (FynSH4U). The arrows (bottom panel) indicate the direction of movement of migrating cells. (C) The translocation of induced kinases can be quantified by comparing kinase intensity in different regions of cells at a given time point. Error bars indicate 90% confidence intervals (n>55 cells). Rapamycin was added at time zero to activate the engineered kinases. (D) The graph shows the percentage of cells responding for each behavior over time. Rapamycin was added at time zero to activate the engineered kinases. The upper part of the graph shows the percentage of cells considered non-responsive (black).

An intact microtubule cytoskeleton is required for directional movement induced by Src activation

Together, the results of activating Fyn, Src, and their derivatives suggest that the activation of kinases in the perinuclear region is critical to induce polarized movement. The migration of mammalian cells is initiated by a morphological polarization, in which cells form a leading edge at the front of the cell. In many cell types, microtubules are involved in the establishment of morphological polarity required for directional movement (83-86). It has been suggested that microtubule dynamics are responsible for delivering proteins from the Golgi to the leading edge, which provides proteins needed for forward protrusions (87, 88). Therefore, we wanted to test whether the activation of Golgi-localized Src requires microtubules to be targeted to proper locations in order to generate directional movement. To address this question, cells were treated with 10 μM nocodazole, which interferes with the polymerization of microtubules, before activating Src with rapamycin. Interestingly, cells with disassembled microtubules still exhibited Src translocation. This result shows that the release of Src kinases from Golgi compartments is not affected by microtubule disruption. However, instead of inducing directional cell movement upon kinase activation, nocodazole-treated cells protruded in a random manner (Fig. 2.19). This suggests that kinases or other effectors need microtubules in order to be targeted to their proper locations. This result implies that translocation of Src from the Golgi to the periphery is essential to generate directed movement and that microtubule integrity is required for targeting proteins to leading edges.

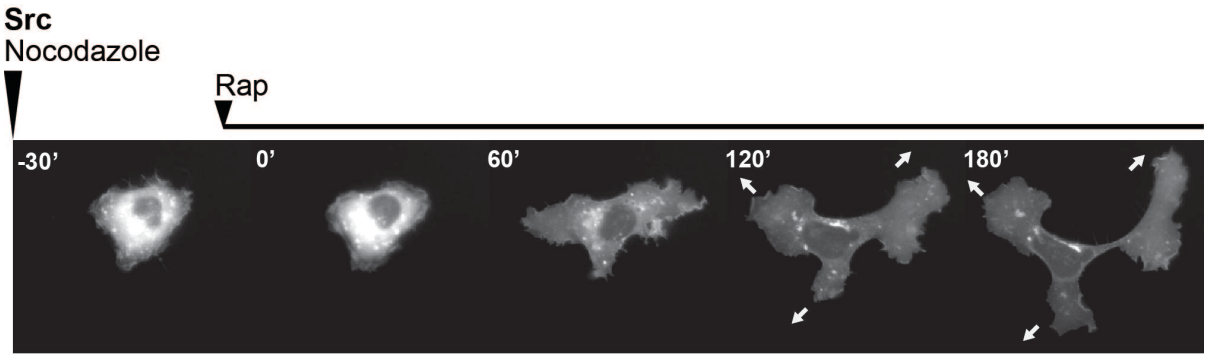

Figure 2.19. Intact microtubules are required for Src-induced polarized movement. Time-lapse fluorescence image of a Cos7 cell expressing EGFP tagged RapR-Src. Cells treated with 10 μM nocadazole for 30 minutes before Src was activated with rapamycin (time zero) and showed multiple protrusions extending with no clear polarization.

Activation of Src, but not Fyn, effectively drives Src to translocate into adhesion sites and facilitate adhesion turnover

Cell migration requires spatiotemporal changes in cell morphology, as well as changes in adhesions to the extracellular matrix (27, 89-92). Src is a critical mediator of adhesion-related signaling that promotes cell motility (33, 93, 94). Fibroblasts lacking *src, fyn,* and *yes* genes show impaired cell migration and adhesion turnover (28). It has been suggested that SFKs activate focal adhesion proteins by phosphorylation to regulate focal adhesion dynamics (59, 95). To examine whether individual SFKs affect focal adhesion dynamics, time-lapse images of cells expressing an adhesion marker, Vinculin, were collected using total internal reflection fluorescence microscope (TIRF). Focal adhesions were identified and quantified using the focal adhesion analysis system (FAAS) (http://gomezlab.bme.unc.edu/tools) (96).

Activation of Src, Fyn, and Fyn Palm$^-$ all led to robust formation of adhesions. However, the adhesion dynamics of palmitoylated Fyn were different than the dynamics of the non-palmitoylated kinases, Src and Fyn Palm$^-$ (Fig. 2.20A). Src and Fyn Palm$^-$ exhibited faster adhesion turnover as compared to Fyn. In figure 2.20B, we analyzed how fast the adhesions disassemble after activation. Around 60 percent of adhesions still remained after 30 mins of activation in cells expressing Fyn; in contrast, adhesion disassembly happened much faster in cells expressing Src and Fyn Palm$^-$. To examine whether Src and Fyn directly act on adhesions, we determined the recruitment of kinases at the adhesion sites by quantifying the kinase intensity at adhesions. Src and Fyn Palm$^-$, but not Fyn, were quickly recruited into adhesions after activation (Fig. 2.20B). These results provide an explanation for the slower adhesion turnover upon Fyn activation. We propose that palmitoylation restrains the cellular distribution of Fyn, causing inefficient translocation into adhesion sites upon kinase activation, resulting in slower adhesion turnover.

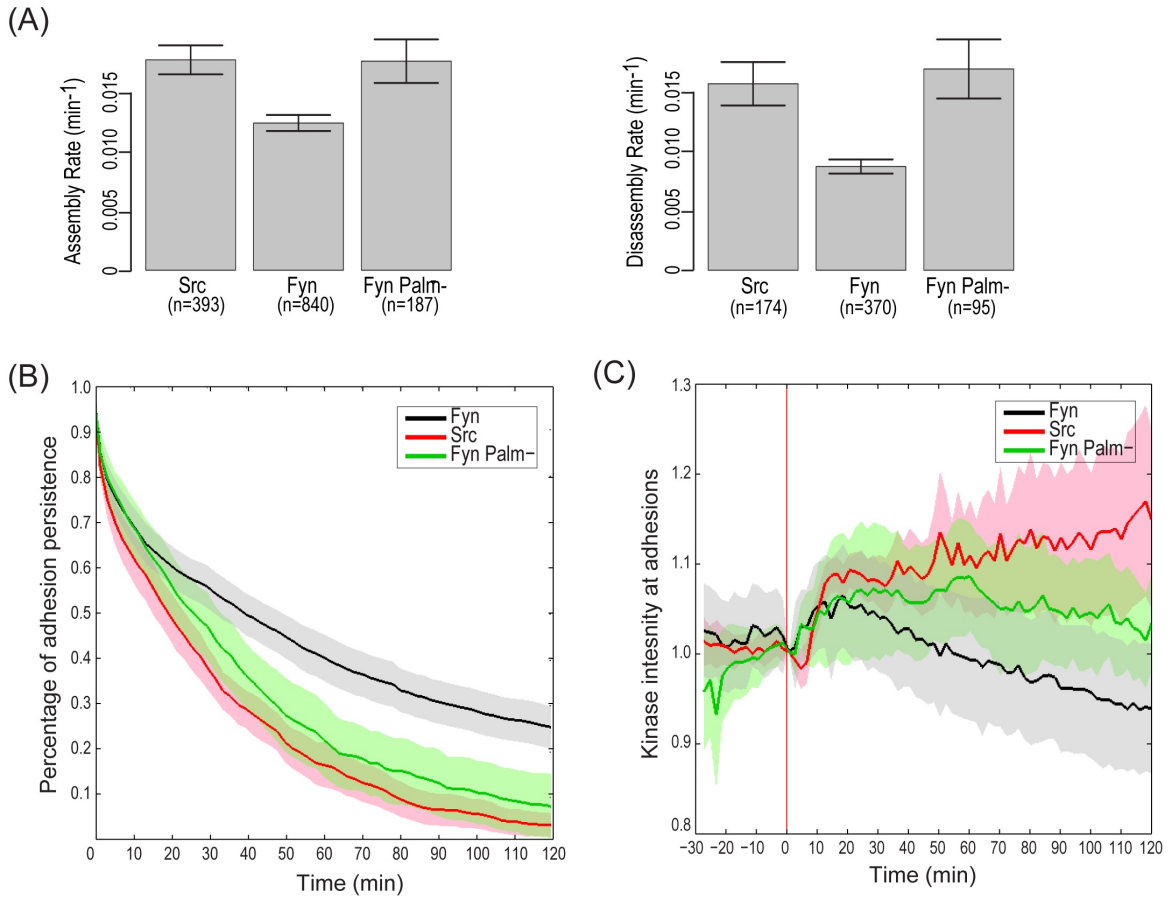

Figure 2.20. Fyn does not effectively translocate into adhesion sites, resulting in slower adhesion disassembly after activation.

(A) Adhesion turnover rates of Src, Fyn, and Fyn Palm$^-$. (B) The persistence of adhesions, plotted as the percent initial intensity of mVenus-tagged vinculin remaining in adhesions over time (shaded regions show 95% confidence intervals, intensity at time of rapamycin addition = 100%) (C) Normalized mean kinase intensity at adhesions over time (shaded region indicates 95% confidence intervals). The vertical red line indicates time of rapamycin treatment. (n>15 cells from two independent experiments)

2.4 Conclusion

Our work not only reveals the distinct morphological changes induced by Src and Fyn activation but also provides insights into which domains contribute to the functional specificity of SFKs in regulating cell motility. First, we generated regulatable kinases for specific Src family members to gain absolute control of individual SFKs. Second, we developed a computational method to automatically characterize cell morphodynamics for a large population of living cells. These complicated cell shape changes could be characterized using two parameters, and the cell behaviors were defined by plotting the measurements onto a parameter space. Third, we revealed that Fyn and Src induce distinct cellular responses during the early stages of activation; prior to this study the immediate responses of specific SFK activation had not been observed. Finally, modified RapR-kinases allowed us to investigate the roles of the functional domains of Fyn and Src in contributing to cell responses induced by kinase activation. These results allowed us to gain insight into the functional specificity and regulation mechanisms of highly conserved Src family members.

Multiple Src family members are expressed in many different cell types and are involved in individual and overlapping signaling pathways. Although distinctive cellular distributions of SFKs have been implicated, their functional specificity and how their subcellular localizations contribute to cell motility were largely unknown. The main contribution of this study is the finding that activation of Fyn and Src induce distinct morphological changes, and that this is mediated by differences in lipid-modulated subcellular localization. The RapR strategy, combined with the computational methods developed in this study, provides temporal resolution when characterizing morphological changes and kinase distribution (Fig. 2.21). The spreading phenotype induced by both Fyn

and Src happen immediately after kinase activation and do not require kinase translocation. Therefore, the spreading phenotype is likely generated by those kinases already associated with the membrane. Polarized movement only occurred in cells expressing kinases that accumulate in the perinuclear region, such as Src and Fyn Palm$^-$. Additionally, this polarized movement occurred at the later stage of kinase activation, after the kinases were released from the perinuclear region and translocated into adhesions (Fig. 2.21A and B). These results imply that the polarized behaviors may take place after the important effectors, which are located at the perinuclear region, have been activated by the kinases (Fig. 2.21C). Experiments using nocodazole, to disrupt microtubules, suggest that targeting kinases or other important effectors to the proper location is essential for generating directional movement.

Based on these results, we propose a model to explain the different cellular responses induced by Fyn and Src activation (Fig. 2.22). Activation of both membrane-associated Fyn and Src initially induce cell spreading. However, only Src activation generates polarized movement through regulating the key components, which are involved in cell polarization and are located at the perinuclear region, by Src accumulated at the perinuclear region. Our findings support the hypothesis that the distinct localizations of Fyn and Src are critical for functional specificity, as they allow Fyn and Src to interact with different substrates. This hypothesis is further supported by experiments that show that changing the cellular distribution of Fyn into that of Src is sufficient to convert the cellular responses. Although several studies have reported the differences in localization and trafficking pathways for individual SFKs (79, 97-99), our work is the first showing that distinct localization of SFKs is responsible for inducing different cellular responses. Future studies that use the RapR-

kinases to identify substrates specific for individual SFKs will provide more detailed insights into the mechanisms of how individual SFKs regulate different signaling pathways.

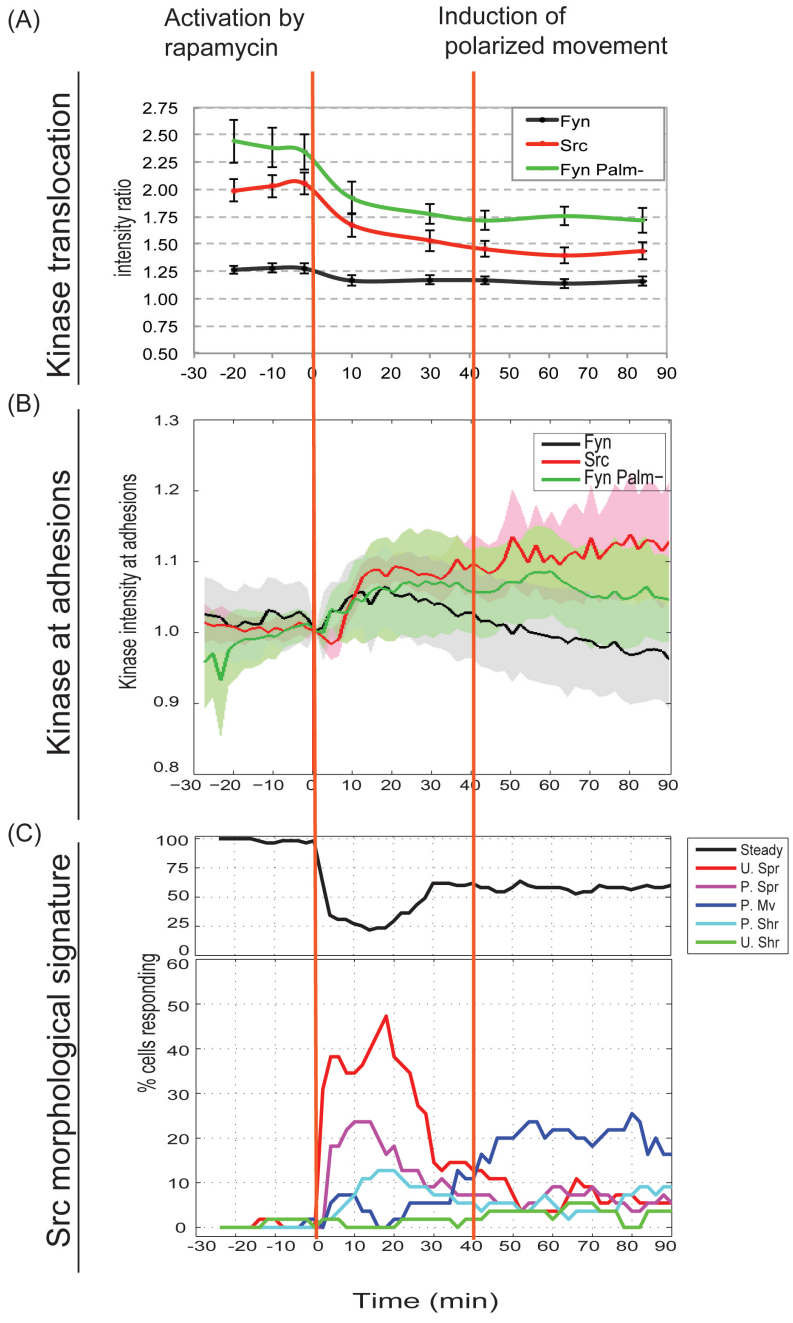

Figure 2.21. The RapR strategy reveals immediate effects of specific kinase activation and provides temporal information during the activation process.

The RapR strategy reveals immediate effects of specific kinase activation and provides temporal information during the activation process. (A) Both Src and Fyn Palm$^-$ showed perinuclear sequestration and dispersion after kinase activation. Induction of polarized behaviors happened after kinase dispersion and reached equilibrium after forty minutes. The translocation of kinases can be quantified by comparing kinase intensity in different regions of cells (intensity ratio) at a given time point. Error bars indicate 90% confidence interval (n>55 cells). (B) The timing of kinase translocation to adhesions correlated with those of kinase dispersion events. Normalized mean kinase intensity at adhesions over time (shaded region indicates 95% confidence interval; n>15 cells from two independent experiments). (C) Activation of Src, Fyn and Fyn Palm$^-$ all resulted in uniform spreading. The polarized movement induced by Src activation was initiated after kinase translocation (Fig. 2.21A) and after the kinases translocated into adhesions (Fig. 2.21B). The graph shows the percentage of cells responding for each behavior over time (n>55 cells). Rapamycin was added at time zero to activate the engineered kinases (red line on the left). The polarized movement was induced around forty minutes after kinase activation (red line on the right).

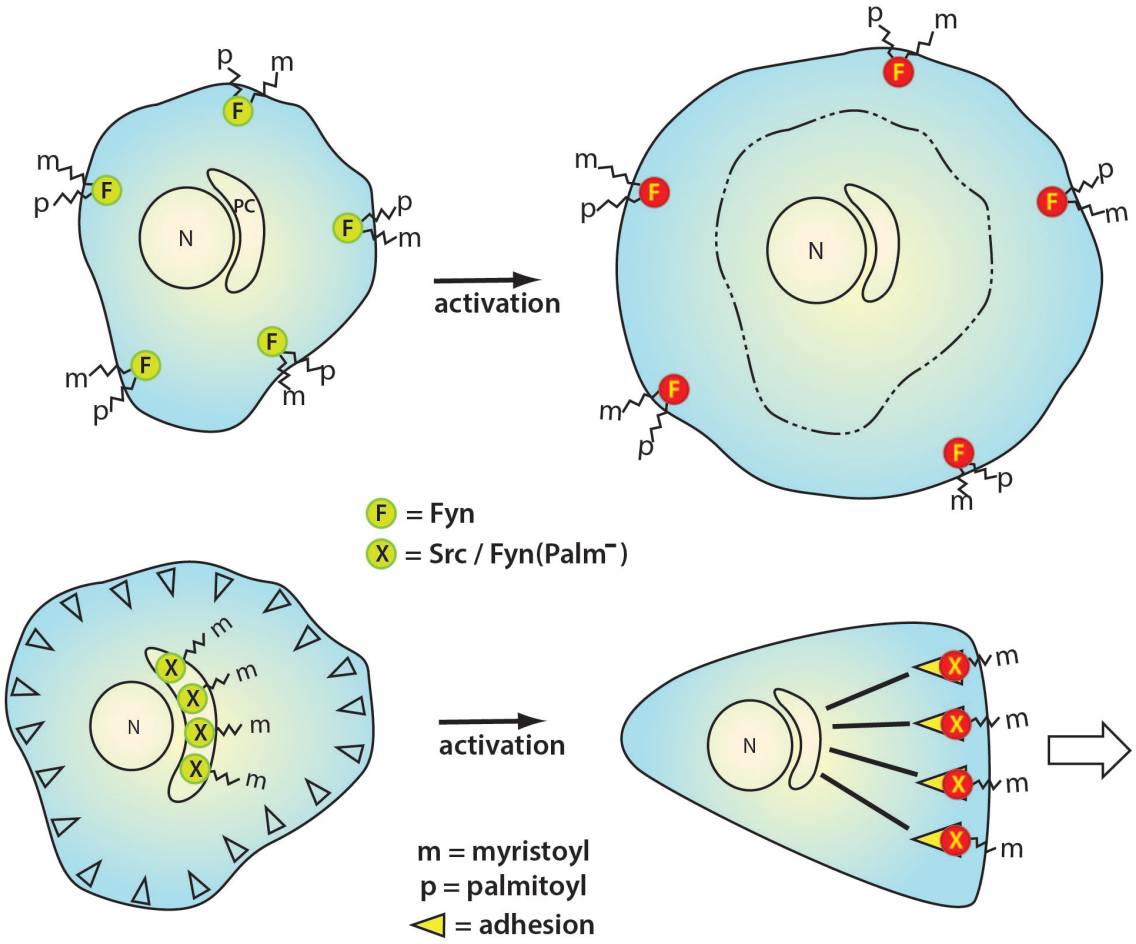

Figure 2.22. Model for spatio-temporal control of Fyn and Src activity.

Activation of Src or Fyn initially leads to uniform spreading, likely due to the presence of these kinases at the cell boundary. Because it is palmitoylated, Fyn is localized at the boundary and not the perinuclear compartment. Wild type Src, which has no palmitoyl, is initially localized at a perinuclear compartment. When they are released from this compartment, traveling via microtubules to one portion of the edge, that portion protrudes preferentially, becoming the leading edge of a polarized, moving cell. Only the proteins that show the sequestration and release travel to adhesions at the cell edge and increase adhesion turnover.

2.5 Materials and Methods

Antibodies and reagents

The following antibodies were used in these studies: anti-Myc (Millipore), anti-GFP (Clontech), anti-phospho-Paxillin (Tyr31) (Invitrogen). IgG-coupled agarose beads were purchased from Millipore and glutathione agarose resin was purchase from Pierce. Rapamycin was purchased from Sigma. All restriction enzymes were purchased from New England Biolabs.

Cell culture and transfection

293 LinXE and COS-7 cells were cultured in Dulbecco's Modified Eagle Medium (DMEM) supplemented with 1% GlutaMax^{TM} (Invitrogen) and 10% FBS. To generate cells expressing RapR-kinases and FRB, cells were transfected using Fugene$^{®}$6 reagent (Promega) following the manufacturer's protocol.

Construction of RapR-kinases specific for Fyn, Yes, and Lyn

Human Fyn, Yes, and Lyn were cloned into the pUSE-EGFP-Myc plasmid using NheI/AscI cloning sites. The insertable FKBP (iFKBP) domain was derived from human FKBP12, comprising amino acids Thr22 through Glu108 of FKBP12. Insertion of iFKBP in the middle of the Fyn, Yes, and Lyn genes was performed using a method modified from the Stratagene Quickchange site-directed mutagenesis protocol (100). The iFKBP inserts were amplified by PCR such that their 5'- and 3'-end sequences annealed at the desired insertion site within the Fyn, Lyn, and Yes genes. The PCR products were used as mega-primers for site-directed

mutagenesis reactions. In the RapR-Fyn constructs, the iFKBP inserts contained various combinations of linkers on the left/right sides and are listed as followed: PG/GPG, GSPG/GPG, GS_2PG/GPG and GS_3PG/GPG. The linker GPG/GPG was used to flank iFKBP and inserted in both Yes and LynA to generate RapR-Yes and RapR-LynA. The FRB domain of human FRAP1 protein was cloned into the pmCherry-C1 vector using EcoRI/BamHI cloning sites.

Generation of Src and Fyn derived RapR-kinases

The Fyn $Palm^+$ (C3SC6S mutant Fyn) and Src $Palm^-$ (S3CS6C mutant Src) constructs were generated using the modified site-directed mutagenesis method described above. Src (FynSH4U) was prepared by replacing SH4 and Unique domains of Src (1-82) with the SH4 and Unique domains of Fyn (1-81). To generate Src (FynSH32) and Fyn (SrcSH32), overlap extension PCR methods were used to generate SrcSH3SH2 domain (Gly83 to Cys253) or FynSH3SH2 domain (Thr82 to Cys246) and inserted into the corresponding site of RapR-Fyn or RapR-Src to replace their original domains.

Immunoprecipitaion and kinase assays

Myc-tagged RapR-kinases and FRB were co-expressed in 293 LinXE cells. The expressing cells were treated with 500 nM rapamycin or equivalent volume of ethanol (control) for 1 hour in the incubator. Cells were then washed with cold-PBS and lysed with lysis buffer (20 mM HEPES-KOH, pH 7.8, 50 mM KCl, 100 mM NaCl, 1 mM EGTA, 1% NP40, 1 mM NaF, 0.1 mM Na3VO4) containing 250 nM rapamycin or an equivalent volume of ethanol corresponding to their treatment. Cell lysates were clarified by centrifugation at 3,000 × g for

10 min at 4 °C. Cleared cell lysates were incubated with IgG-linked agarose beads prebound with anti-Myc antibodies for 2 hr at 4 °C for immunoprecipitation. The beads were washed two times with wash buffer (20 mM HEPES-KOH, pH 7.8, 50 mM KCl, 100 mM NaCl, 1 mM EGTA, 1% NP40) and two times with kinase reaction buffer (25 mM HEPES, pH7.5, 5 mM $MgCl_2$, 5 mM $MnCl_2$, 0.5 mM EGTA). The immunoprecipitates were resuspended in kinase reaction buffer. Kinase assays were carried out at 37 °C for 10 min with 20 µl precipitates in the presence of ATP, and the purified N-terminal fragment of Paxillin was used as a substrate. The reactions were stopped by adding 2x Laemmli protein sample buffer.

Live cell imaging

For cell morphology studies, COS-7 cells expressing EGFP-tagged RapR kinase and mCherry-tagged FRB were used in the experiments. Cells were plated on fibronectin-coated coverslips (5ug/ml fibronectin) 2 hr before the experiment, then transferred to L-15 medium (Invitrogen) supplemented with 5% FBS. Rapamycin was added into the medium 30 min after imaging. Live cell imaging was performed in an open heated chamber using an Olympus IX-81 microscope equipped with an UPlanFLN 40X objective (Oil, NA 1.30). Image analysis was performed using Metamorph software and Matlab. For focal adhesion studies, COS-7 cells expressing CFP-tagged RapR kinase, mCherry-tagged FRB and mVenus-tagged vinculin were used in the experiments. Live cell imaging was performed using an Olympus IX-81 microscope equipped with an objective-based total internal reflection fluorescence (TIRF) system and a PlanApo N 60X TIRFM objective (NA 1.45). Time-lapse movies were taken at 2 minutes time intervals. All images were collected using a Photometrics CoolSnap ES CCD camera.

Quantification of morphological changes

All morphometric quantifications were based on fluorescence intensities generated from imaging COS-7 cells expressing EGFP-tagged RapR kinases. The analysis was performed using a MATLAB-based Graphical User Interface (GUI) specifically designed for this project. The processing involves two steps. The first step is cell boundary detection using the *MovThresh* module that automatically finds intensity thresholds for each time frame of the loaded movie. The GUI also provides options for manual adjustment of the threshold value. The second step is the motion type classifier using the *Squigglymorph* module. This module finds and displays regions of protrusion and retraction by pairwise comparison of cell boundaries at time frames t and $t+T$, where T is the user-defined time lag. The distribution of protruding boundary points is illustrated by mapping an arbitrarily shaped cell boundary on a circle and quantified with a polarization vector, $\vec{p}(t)$, according to the equation:

$\vec{p}(t)=(p_x,p_y)=\left(\int_0^{2\pi} d(a)\cos(a)\,\mathrm{d}a,\int_0^{2\pi} d(a)\sin(a)\,\mathrm{d}a\right)$, where a is the angular coordinate of the boundary point on the circle and $d(a)$ is the corresponding displacement of the boundary point between time t and $t=T$. For the polarization index, $P(t)=\sqrt{\langle p_x\rangle^2+\langle p_y\rangle^2}$, we used the running average of three polarization vectors from consecutive time points, which accounts for the persistence of the polarization. The polarization index and the rate of area change, $R(t)=dA/dt$, form the phase space that splits into 6 regions corresponding to the uniform spreading $(P<P_{cr},R>R_{cr})$, polarized spreading $(P\geq P_{cr},R>R_{cr})$, uniform shrinking $(P<P_{cr},R<-R_{cr})$, polarized shrinking $(P\geq P_{cr},R<-R_{cr})$, polarized movement $(P\geq P_{cr},|R|\leq R_{cr})$, and the unchanged state $(P<P_{cr},|R|\leq R_{cr})$. This way at each time point the

cell is characterized as being in one of the 6 possible modes of motion and the cell dynamics are visualized as a trajectory in the phase space. The critical parameters P_{cr} and R_{cr} were adjusted in order to provide the best correspondence between visually determined behavior and the program output. In this case, P_{cr} =0.28 and R_{cr} =0.005. Batch processing of all cells for each construct (n>55 cells) were collected for statistical results. Additional features of *Squigglymorph* include 1) the construction of smoothed curves for the parameters $P(t)$ and $R(t)$ with the user-defined size of the smoothing window; and 2) calculation of the mean squared displacement (MSD) of the cell centroid and fitting the resulting curve with the persistent random walk equation in order to make an estimate for the centroid speed and persistence (80, 81): $MSD=\langle d^2(t)\rangle=2S^2P[t-P(1-e^{-t/P})]$. The direction persistence time, P, was obtained by MSD analysis over 3 hours.

Focal adhesion dynamics

The mVenus-Vinculin-labeled focal adhesions were segmented and tracked as previously described (96). We used a threshold of four standard deviations to segment the adhesions. To measure the localization of the kinase constructs, we found the average intensity of the kinase channel within each adhesion and then averaged these values to summarize the relative intensity of the kinase at the adhesions. To minimize cell-to-cell variability, we normalized the average kinase intensities to one in the image immediately before kinase activation. Adhesion turnover was quantified by measuring how quickly the adhesions present at kinase activation disappeared from the cell. This value is expressed as the percentage of adhesions still present after kinase activation.

CHAPTER THREE: LIGHT-INDUCED INHIBITION OF SRC VIA LOV DOMAIN INSERTION INTO A CONSERVED PORTION OF THE CATALYTIC DOMAIN

3.1 Overviews

Src is a non-receptor tyrosine kinase that participates in a diverse spectrum of signaling pathways. The interactions of Src with activators and downstream ligands depend on the spatio-temporal dynamics of Src activation; it would therefore be valuable to be able to control the timing and location of Src activation *in vivo*. To gain spatiotemporal control of protein activity in living cells, we utilized a protein domain, the light oxygen voltage (LOV) domain, from a photosensory protein to generate light-regulatable Src. By inserting the LOV domain into a conserved portion of the catalytic domain of the kinase, we generated a genetically encoded analog of Src (photoinhibited Src, or PI-Src) that is reversibly inhibited upon irradiation at wavelengths between 400 and 500 nm. Molecular dynamics studies indicate that the light-induced unwinding of the LOV Jα-helix results in the narrowing of the ATP binding site. This causes the activation loop and the glycine-rich loop to move closer to each other, generating an inactive Src structure. Insertion of the LOV domain with an optimized linker minimally perturbed Src catalytic activity in the dark, but led to a reduction in activity upon irradiation. Src inhibition by light resulted in a reduced migration rate and decreased frequency of protrusions in fibroblasts expressing PI-Src. The transforming phenotypes induced by expressing PI-Src in the dark were reverted to normal phenotypes

upon irradiation. Structural studies and insertion of other engineered folds into the same Src site indicate that this strategy can be broadly applied to other kinases.

3.2 Introduction

Design of LOV domain photoswitches

Src kinase plays an important role in regulating cytoskeleton dynamics and cell motility. Cell migration is critical for immune responses, developmental processes in normal cells, and even cancer cell metastasis. While evidence has shown that Src has prominent roles in cell motility, it remains unclear how Src regulates the coordination of cell polarization, cytoskeleton rearrangement, and adhesion dynamics to promote migration. Precise spatial and temporal coordination of molecular events is critical for generating cell behaviors. I demonstrated in chapter 2 that we were able to use small molecules to provide precise temporal control of kinase activity. However, it remains difficult to manipulate protein activity at specific locations within living cells using this approach. To generate a tool that can specifically and spatially control protein activity, a photosensory protein was used to enable optical control.

Phototropins are light-activated photosensory protein kinases that control a wide range of responses in plants, including phototropism, chloroplast migration, and stomatal opening (101). Photosensory events are achieved through protein domains that bind light-absorbing chromophores and convert photon energy into structural change (102). In this study, we used the LOV2 (light, oxygen, and voltage) domain from *Avena sativa* phototropin 1 as a light-induced switch. The LOV domain, which is regulated by external signals, is composed of a Per-ARNT-Sim (PAS) motif adjacent to a helix (Jα). Upon 400-500 nm

illumination, the flavin chromophore forms a covalent adduct with a conserved cysteine residue in the PAS motif, which results in the unwinding of the C-terminal Jα helix (103, 104). The significant conformational change and the spontaneous reversibility make the LOV domain an excellent molecular switch for regulating protein activity (105). Previous studies have used the LOV domain to allosterically control protein activity, as demonstrated using the *Escherichia coli* Trp suppressor (LOV-TAP) (106), a small GTPase Rac1 (PA-Rac) (107), and dihydrofolate reductase (DHFR) (108) in mammalian cells. The first two were generated as end-to-end fusions of the LOV domain to the proteins of interest. In the case of LOV-TAP, the LOV domain was fused to the N terminus of the Trp protein, via a helix extending from the Jα-helix, to generate a steric domain-domain overlap. Light-induced undocking of the Jα-helix from the LOV core domain results in an increase in the affinity of DNA binding to the Trp domain. Strickland *et al.* proposed that the Jα-helix of the LOV domain acts as a lever arm, connecting the LOV core domain and Trp protein. The light-induced change of the LOV domain causes a global shift in the conformational ensemble, driving the Trp domain into the active conformation. In the application of photoactivatable Rac1 (PA-Rac), the LOV domain sterically blocks the interaction of Rac1 and its effectors until light-induced unwinding of the Jα-helix relieves the steric inhibition. Lee *et al.* used a different approach to design photoactivatable DHFR. They inserted the LOV domain into sites identified using statistical coupling analysis, as allosterically active regions of the protein. The allosteric communication between the LOV domain and DHFR drives the light-dependent activation of this chimeric protein. To summarize, the advantages of LOV domain based-photoswitches are: (1) the size of LOV domain is small (~15 kDa), providing better solubility and less toxicity, (2) the mechanism of light-induced conformational changes is

well-characterized, (3) the photoreaction is reversible, and (4) the essential chromophore (flavin) is ubiquitously expressed and found in cultured cells and cells within animals.

3.3 Results and Discussion

Development and validation of photo-regulatable Src using the LOV domain

To gain localized control of Src activity, we decided to use the LOV domain as a molecular switch to generate a photo-regulatable Src. We previously demonstrated that insertion of iFKBP in the catalytic domain of Src allowed us to generate a rapamycin-regulatable Src (RapR-Src), as described in this thesis above. From the development of RapR-Src, we learned that insertion of iFKBP into the insertion loop, which is proximal to the G-loop, disrupts the catalytic activity of Src. In the presence of rapamycin, the FRB protein can form a tight complex with iFKBP, causing conformational changes. This conformational change is propagated to its adjacent position, the G-loop. Structural studies have shown that the flexibility of the G-loop is critical for the catalytic activity of tyrosine kinases (67). Together, these results suggest that by modifying the insertion loop we can control the structural stability of the G-loop, thereby controlling Src activity. Therefore, we proposed building a photo-regulatable Src by inserting the LOV domain into the insertion loop of the Src catalytic domain (Fig. 3.1B).

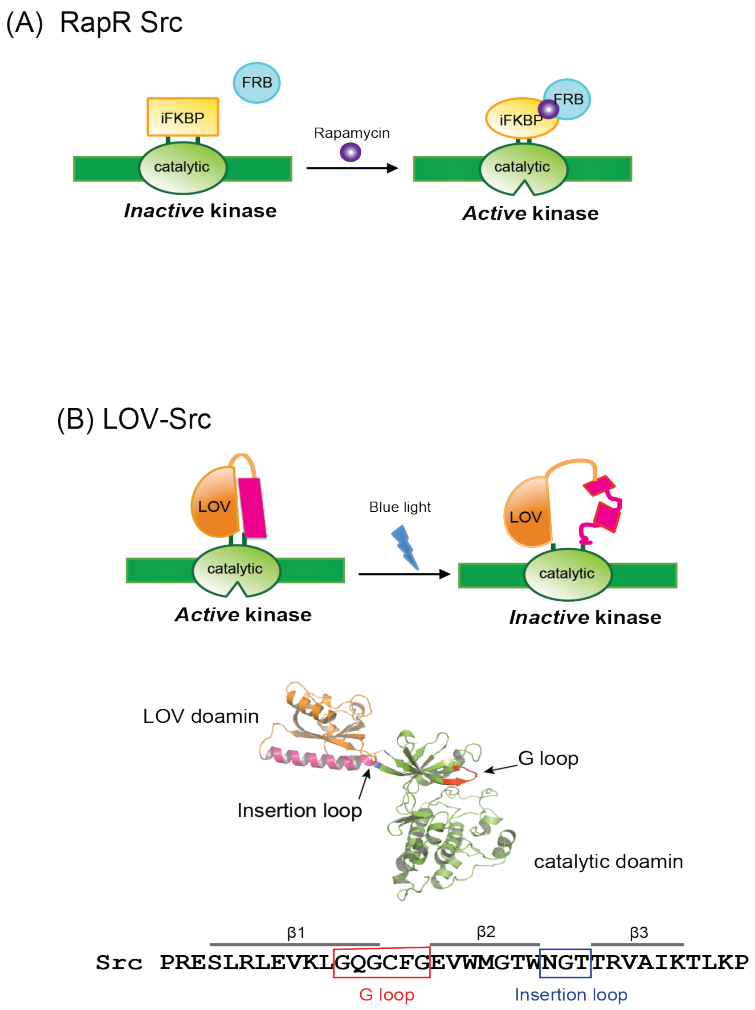

Figure 3.1. Insertion of the FKBP and LOV domains into the same position of Src allows allosteric control of Src kinase activity by rapamycin and light.

(A) Schematic representation of rapamycin-induced activation of RapR-Src catalytic activity. (B) Schematic representation of photo-stimulation of the LOV domain to regulate the catalytic activity of LOV-Src. The LOV domain is inserted into the insertion loop, which is linked to the G-loop by a β-strand.

To optimize the regulation of kinase activity through the LOV domain, we replaced the glycine in the insertion loop (amino acid sequence NGT) with the LOV domain (Leu404-

Leu546) using different linkers (Fig. 3.2A). The effects of the LOV domain conformational changes on LOV-Src kinase activity were tested using LOV domains with mutations mimicking the dark and lit states of the LOV-Src fusion proteins. The dark mutation (C450M) in the LOV domain prevents chromophore adduct formation and generates a "dark-state" of the LOV domain, while the lit mutations (I539E/I510E) in the LOV domain disrupt the interaction between the PAS motif and the Jα helix to create a "lit-state". Kinase activity was determined using an anti-phosphotyrosine (p-Tyr) antibody to analyze the profiles of phosphotyrosine-containing proteins in cells expressing LOV-Src variants. Without the LOV domain insertion, cells expressing constitutively active Src (Src CA) displayed elevated levels of phosphotyrosine-containing proteins (p-Tyr). Inserting the lit mutant LOV domain into Src CA abolished the kinase activity and resulted in decreased levels of p-Tyr proteins, as compared to Src CA with the dark mutant LOV domain insertion. Testing various linkers we found that the LOV domain insertion using the GPG linker showed a larger difference in the phosphorylation profiles between the constructs with the dark and lit mutant LOV domains. This result suggests that inserting the LOV domain into Src using the GPG linker provides better control of kinase activity through LOV domain conformational changes. Therefore, LOV-Src, inserted with the GPG linker, will be used in later studies. We refer to this construct as photoinhibitable Src (PI-Src).

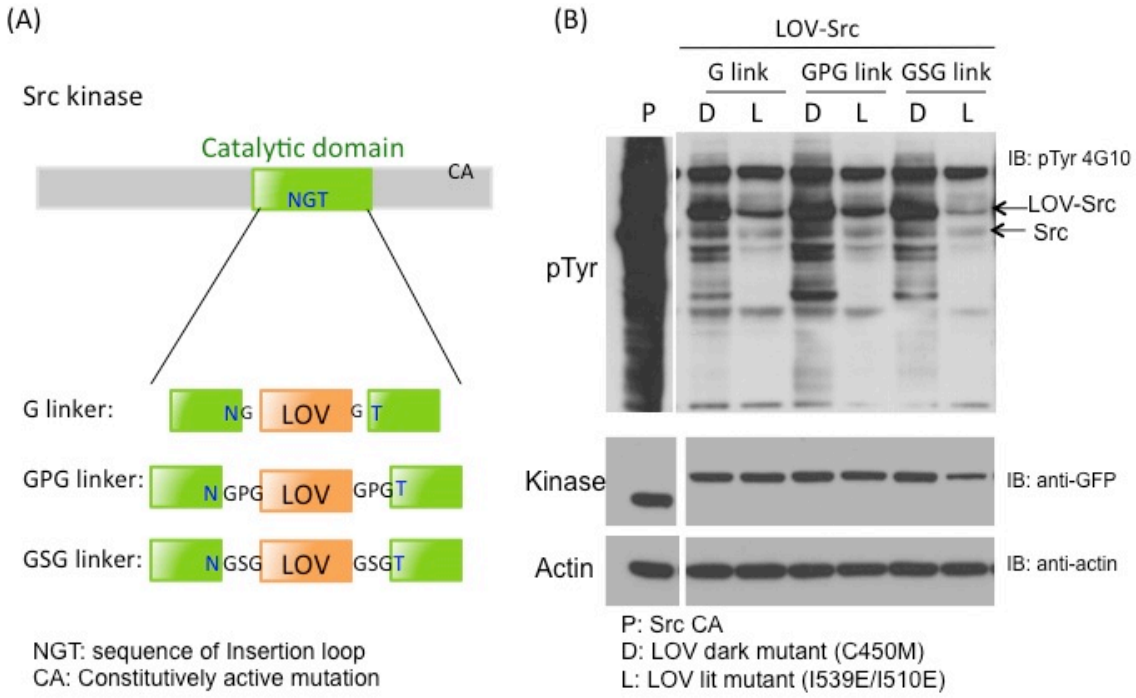

Figure 3.2. Biochemical characterization of LOV-Src kinase.

(A) Schematic representation of the LOV domain insertion. The glycine residue in the insertion loop (amino acid sequence shown in blue) was replaced with the LOV domain, flanked by various linkers. (B) The effects of LOV domain conformational changes were compared using cells expressing LOV-Src constructs containing the dark mutant (D) of LOV domain and the lit mutant (L) of LOV domain. Kinase-induced phosphorylation of substrates was evaluated by immunoblotting using an anti-phosphotyrosine antibody (pTyr).

To further investigate the regulation of PI-Src in living cells using light, the wild-type LOV domain, instead of lit or dark mutant LOV domains, was used to generate PI-Src. Cells expressing controls and PI-Src were cultured with or without light. The kinase activities in dark and lit culture conditions were analyzed by blotting cell lysates for pTyr. The results show that the kinase activities of the positive and negative controls were not affected by light

exposure. However, the kinase activity in cells expressing PI-Src was inhibited by light (Fig. 3.3).

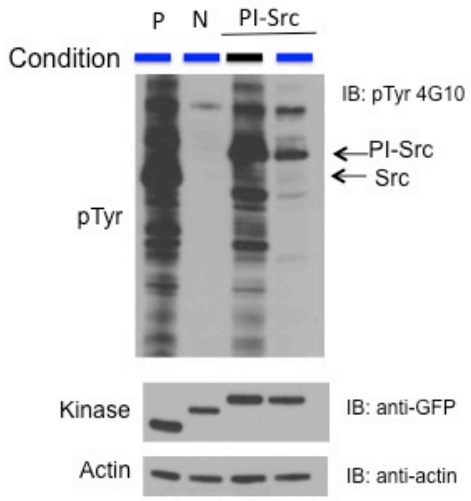

Figure 3.3 The kinase activity of PI-Src can be regulated by blue light irradiation. 293 LinXE cells expressing PI-Src were cultured either in the dark (black bars) or under blue light illumination (blue bars). The pTyr blot represents the kinase activity in cells. Constitutively active Src was used as positive control (P) and a kinase-dead Src mutant was used as a negative control (N). Protein levels of fluorescently tagged kinases were detected by SDS-PAGE and immunoblotting with an anti-GFP antibody. Equal protein loading was determined using an anti-β-actin antibody.

Photoinhibition of PI-Src induces reversible morphological changes

To study Src inhibition in living cells, we expressed constitutively active Src (Src CA), kinase inactive Src (Src KD), or PI-Src in mouse embryonic fibroblast cells lacking three ubiquitously expressed SFK members: Src, Yes, and Fyn (SYF). SYF cells were used in this study to avoid the functional compensation from other endogenous Src family kinases. It has been reported that expression of Src CA mutant is sufficient to induce cell

transformation, resulting in altered cell growth and morphology. Cells transformed by Src CA exhibit a less adherent and less well-spread phenotype than cells expressing Src KD. Thus, we used cell morphology to assay Src activity in living cells. We found that SYF cells stably expressing Src CA or Src KD displayed different morphologies as previously reported in the literature. Expression of PI-Src in the dark resulted in constant activation of Src and generated morphologies similar to cells expressing Src CA. Both positive and negative controls (Src CA and Src KD, respectively), without the LOV domain insertion, did not change their cell morphologies upon light irradiation. In contrast, cells expressing PI-Src exhibited a reversion of cell morphology, resulting in a well-spread phenotype upon light exposure, similar to the negative control (Src KD) (Fig. 3.4).

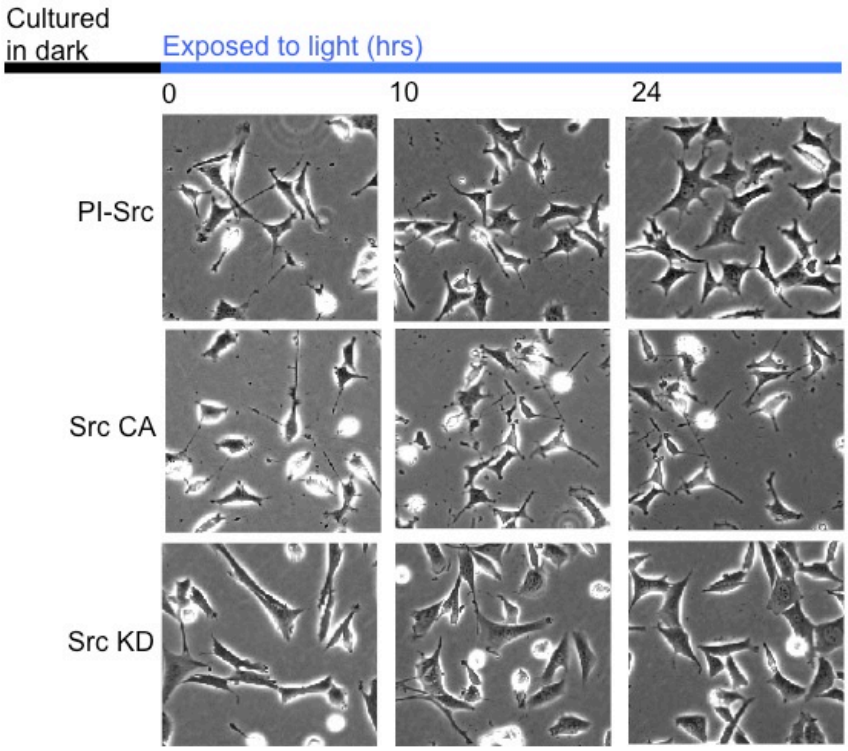

Figure 3.4. Photoinhibition of PI-Src induces morphological changes in living cells.

SYF cells stably expressing PI-Src, Src CA, or Src KD were exposed to light for 0, 10, and 24 hours. Cell morphology was evaluated by phase-contrast microscopy (magnification, X100).

We next investigated whether light inhibition of Src affected the levels of p-Tyr proteins over time. Cell lysates, obtained from SYF cells expressing Src derivatives under light exposure for 0 to 24 hours, were analyzed by western blot with a p-Tyr antibody. While light-irradiation did not affect the kinase activities of controls (Src CA and Src KD), we found a decrease in p-Tyr levels upon light irradiation in cells expressing PI-Src (Fig. 3.5).

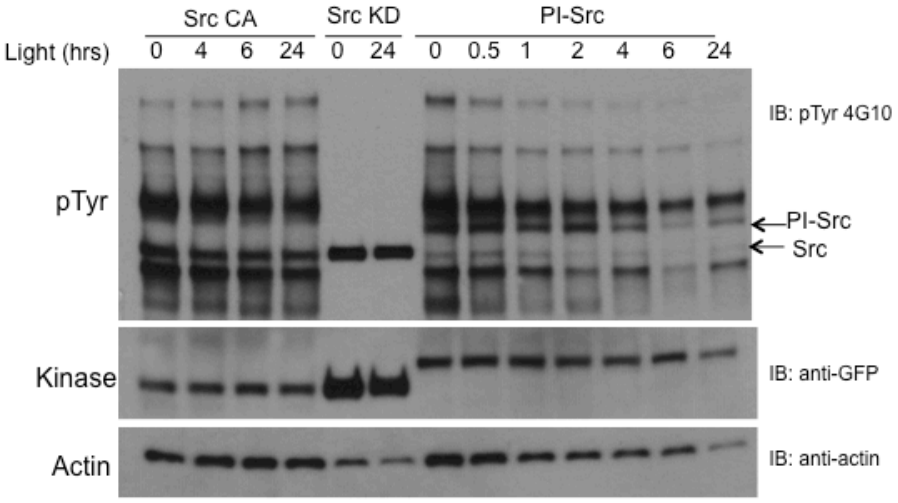

Figure 3.5. Inhibition of Src activity through irradiation causes a decrease in tyrosine phosphorylation levels

SYF cells expressing Src CA, Src KD, and PI-Src were exposed to light for 0 to 24 h, and kinase activity was analyzed using an anti-pTyr antibody. Protein levels of fluorescently tagged kinases were detected by SDS-PAGE and immunoblotting with an anti-GFP antibody. Equal protein loading was determined using an anti-β-actin antibody.

The formation of the light-induced adduct of the LOV domain is fully reversible in darkness, returning the LOV domain back to its initial ground state within tens to hundreds of seconds, depending on the LOV isoform, incorporation of mutations, and its role in specific proteins (109). Therefore, we next examined whether the light-dependent allosteric control of the PI-Src protein can recover when returned to the darkness. Cells stably expressing PI-Src, Src CA, and Src KD were placed on fibronectin-coated glass and cultured under blue light for 24 hours, then returned to the dark for up to 24 hours. Cells expressing Src CA or Src KD did not respond to the light exposure cycle, and retained their original cell shapes. After light illumination cells expressing PI-Src exhibited cell morphologies similar to cells expressing Src KD. These cells, due to the low levels of Src activity, were well-spread and more adherent to the matrix. However, when returning these illuminated cells to the dark, the light-inhibited Src activity was recovered and cells once again displayed rounded and less adherent morphologies, consistent with cells with high Src activity (Fig. 3.6). This result suggests that inhibition of the catalytic activity of PI-Src by light is reversible simply by culturing cells in darkness. The reversibility of cell morphology by inhibiting Src activity is consistent with the effects of using a general tyrosine inhibitor to treat fibroblasts expressing active Src (110). Our strategy clearly demonstrates that Src inhibition is specific and sufficient to revert the cell transformation phenotype. This non-invasive and selective inhibition of Src activity will lead to a better understanding of the cellular consequences resulting from Src inhibition.

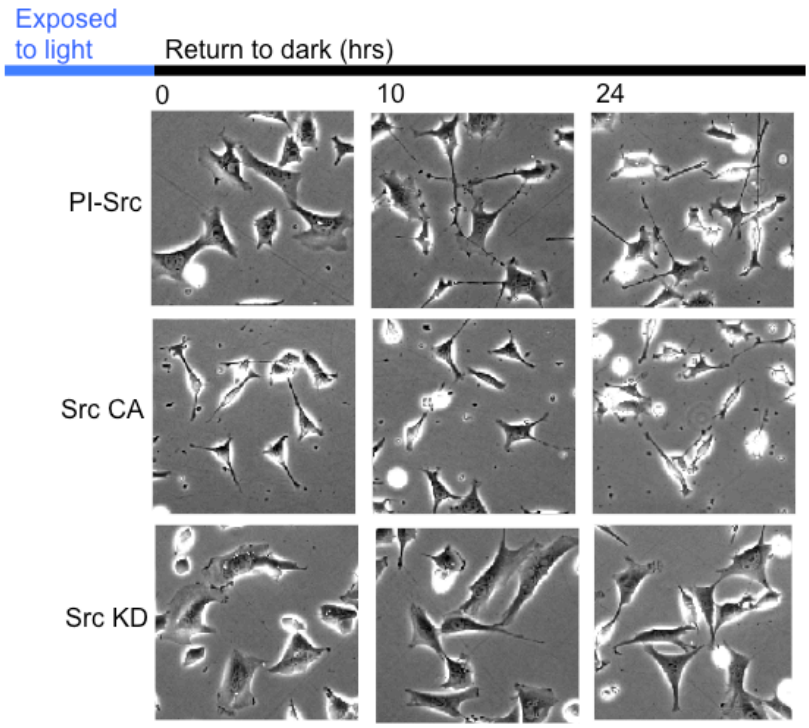

Figure 3.6. Photoinhibition of Src activity can be reversed by culturing cells in the dark.

SYF cells stably expressing PI-Src, Src CA, and Src KD were placed on fibronectin-coated glass and exposed to light for 24 hours. Cells were then returned to the dark. Cell morphology was evaluated by phase-contrast microscopy and images were taken at 0, 10, and 24 hours (magnification, X100).

Photoinhibition of PI-Src results in slowed migration rates

In addition to investigating the changes in cell morphology, we wanted to examine whether Src inhibition by light can alter cellular processes such as cell migration. It is well known that Src activation promotes cell migration. We therefore used SYF cells stably expressing Src variants (PI-Src, Src CA, and Src KD) to determine migration rates under dark or light culture conditions. A scratch wound in a confluent monolayer of cultured stable

cell lines was used to stimulate cell migration, and images were taken at 0 h and 7 h post-wounding time intervals with or without light treatment. The migration rates were compared by examining differences in wound width over time. As shown in Fig. 3.7A, the migration rates of SYFs with Src CA or Src KD were not affected by culture conditions. Cells expressing PI-Src cultured under light exhibited a slow migration rate, whereas cells cultured in darkness exhibited a relatively fast migration rate. This suggests that the insertion of the LOV domain attenuates the catalytic activity of Src in a small degree and that light-induced conformational changes of the LOV domain effectively inhibit cell migration, as a consequence of decreased Src-dependent phosphorylation (Fig. 3.7B).

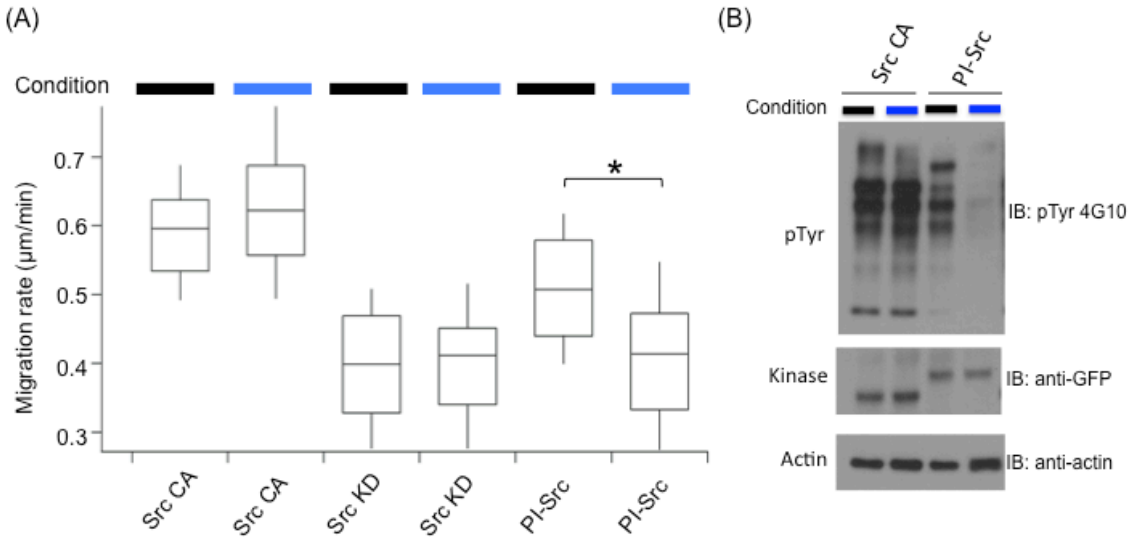

Figure 3.7. Inhibition of kinase activity of PI-Src in SYF cells results in decreased migration rates.

(A) Migration rates were determined by performing wound-healing assays under different culture conditions. (Black and blue bars indicate darkness and lit culture conditions). Means of migration rate displayed as box plots. The bottom and top of each box indicate 25% and 75% quartiles, respectively. Significance value was determined using an unpaired t-test, $p<0.05$. (n=80) (B) Src kinase activity was determined by western blot using an anti-pTyr

antibody. Protein levels of fluorescently tagged kinases were detected by SDS-PAGE using an anti-GFP antibody. Equal protein loading was determined using an anti-β-actin antibody.

Time-course of light-inhibited PI-Src

The cellular responses driven by cytoskeletal rearrangement, such as cell morphological changes and cell migration, require the equilibrium of multiple signaling pathways. Many proteins involved in changing cytoskeletal dynamics are controlled by their phosphorylation states. Therefore, activity of these proteins is directly dependent on the activities of kinases and phosphatases. Turning off activities of these proteins requires inhibition of kinases and activation of phosphatases. In our studies, we use light to turn off the activity of PI-Src in living cells, but the dephosphorylation of phosphorylated substrates are dependent on the activity of phosphatases. Therefore, the equilibrium of kinase and phosphatase has to be taken into account when using the phosphorylation levels of total substrates to measure PI-Src activity. Therefore, to further understand the dynamic regulation of PI-Src by light, we analyzed the effects of light on PI-Src directly, by determining the catalytic activity of illuminated PI-Src using a purified substrate. PI-Src was purified using immunoprecipitation and exposed under full-spectrum light for 0 to 40 mins. The kinase reactions were started by adding an equal amount of purified Paxillin as a phosphorylation substrate. The phosphorylation of purified Paxillin was determined by western blot using an anti-phospho-Paxillin antibody. We examined the effect of light exposure on the catalytic activity of the inactive (Src KD) and active (Src CA) forms of the kinase. Both catalytic activities of Src KD and Src CA were not affected by light. In contrast, the catalytic activity of PI-Src was suppressed by light illumination. PI-Src under long light exposure exhibited

less catalytic activity and resulted in lower levels of phosphorylated Paxillin (Fig. 3.8), while the activity of Src CA remained the same throughout the experiment. Previous studies regarding the kinetics of the LOV domain suggest that the conformational changes happen on a time scale of seconds to minutes. The slow kinetics of PI-Src kinase in this experiment may be due to the source of light (details described in materials and methods) used in this *in vitro* kinase assay. A proper light input, which covers the wavelengths 400- 500 nm and minimizes heat generation, needs to be used to effectively alter the conformation of the LOV domain in order to more robustly inhibit the kinase activity of PI-Src.

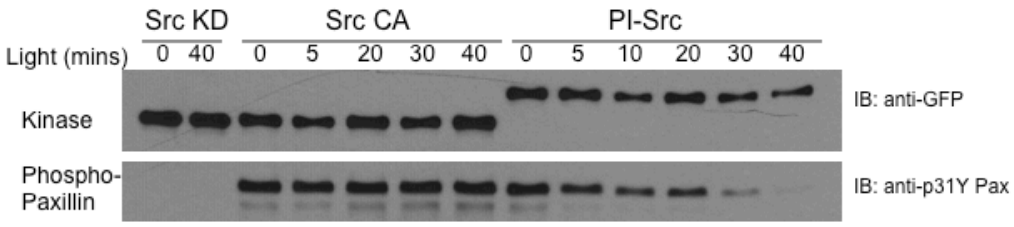

Figure 3.8. Time course of light-mediated PI-Src kinase inhibition.
Purified Src KD, Src CA, and PI-Src were treated with light for the indicated times. The kinase reactions were initiated by adding an equal amount of purified Paxillin to each sample. Phosphorylated Paxillin represents the catalytic activity of the kinases. Protein levels of fluorescently tagged kinases were detected using an anti-GFP antibody.

Src inhibition by light results in cellular contraction

To study the immediate effects of light-mediated Src inhibition, time-lapse images were taken of cells expressing PI-Src under global irradiation. Global irradiation was achieved using a light source for fluorescence excitation that covered the LOV domain absorption wavelengths. In the dark, SYF cells expressing Src CA and PI-Src were motile,

with obvious dorsal ruffles. Upon global light irradiation, only cells expressing PI-Src exhibited reduced membrane ruffling and cellular contraction (Fig. 3.9A upper panel). When returned to the dark, cells expressing PI-Src became motile again and the protrusions recovered. In contrast, cells expressing Src CA were not affected by light and remained motile under the same experimental conditions (Fig. 3.9A, lower panel). To confirm that the contraction phenotype observed in cells expressing PI-Src was not due to the sickness of the cells, we tested the responses of Src inhibition using a Src inhibitor in living cells. PP2 (4-amino-5-(4-chlorophenyl)-7-(dimethylethyl)pryazolo[3,4-d]pyrimidine) has been extensively used in research as a selective inhibitor for Src family kinases (111). However, recent evidence has shown that PP2 non-selectively inhibits many other kinases, besides Src family members (112). Despite this caveat, we wanted to use PP2 to examine what phenotypes are generated by Src inhibition. SYF cells expressing PI-Src, acquired without exposing cells to blue light, are motile with active protrusions before treatment with the inhibitor. Ten minutes after 10 uM PP2 addition to these cells, we observed a contracted response and after thirty minutes the protrusions recovered (Fig. 3.9B). Experiments done in control cells (n=15) did not respond to PP2 treatment. This experiment supports the idea that the cell contraction phenotypes we see are not due to cell sickness caused by photodamage.

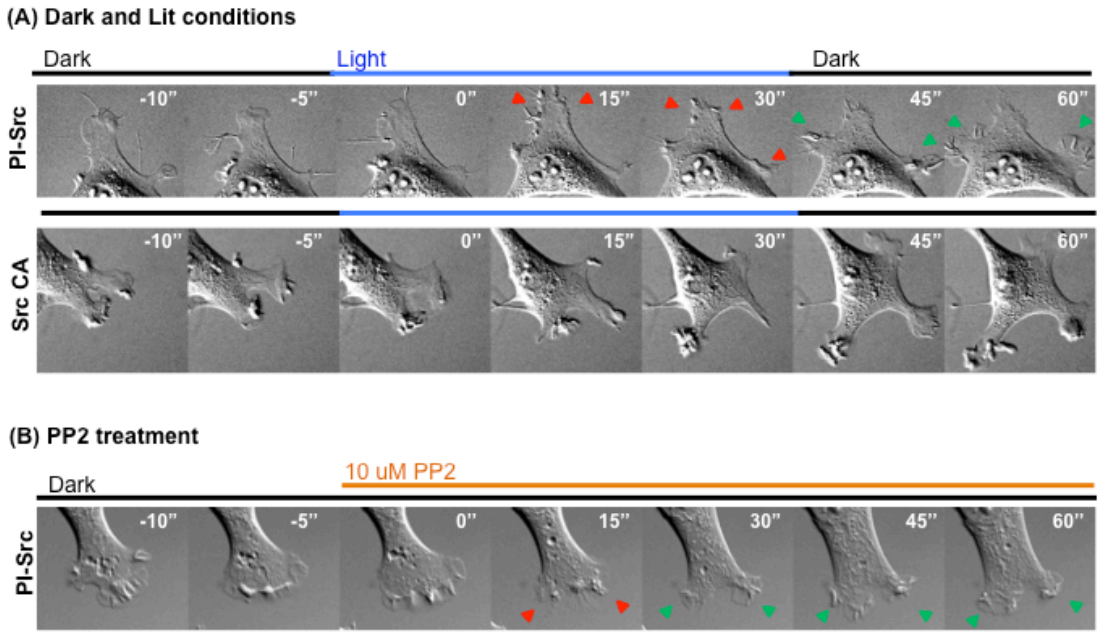

Figure 3.9. Src inhibition by light results in a contraction phenotype similar to that produced by treatment with a Src inhibitor.

(A) Time-lapse imaging of cellular responses of cells expressing PI-Src (upper) or Src CA (lower) under dark and global irradiation cycles. (B) Treatment of SYF cells expressing PI-Src with a Src inhibitor (PP2) show a contracted phenotype similar to cells expressing PI-Src illuminated with light. Red arrows indicate retracted edges and green arrows point to recovered protrusions.

Comparison of the design of RapR-Src and photoinhibited Src

In order to manipulate kinase activity using light, the photosensitive LOV domain was inserted into the Src kinase sequence at the same insertion site where the iFKBP domain was inserted into RapR-Src. Both PI-Src (with the LOV domain insertion) and RapR-Src (with the iFKBP insertion) successfully regulated kinase activity using light or a small molecule, respectively. Previously, a regulatory mechanism of RapR-kinase was proposed

based on the results of molecular dynamics simulations (113-115) (Fig. 3.10A). Comparison of the molecular dynamics of the wild-type kinase and RapR-kinase indicate that insertion of the iFKBP domain into the insertion loop, which is near the ATP binding site, dramatically increases the conformational mobility of the G-loop. However, treatment of rapamycin drives the recruitment of FRB to the inserted iFKBP domain, resulting in subsequent reduction of G-loop fluctuations to wild-type kinase levels, therefore regaining the kinase activity (Fig. 3.10B). These results suggest that modification of the insertion loop enables manipulation of the catalytic activity of kinases.

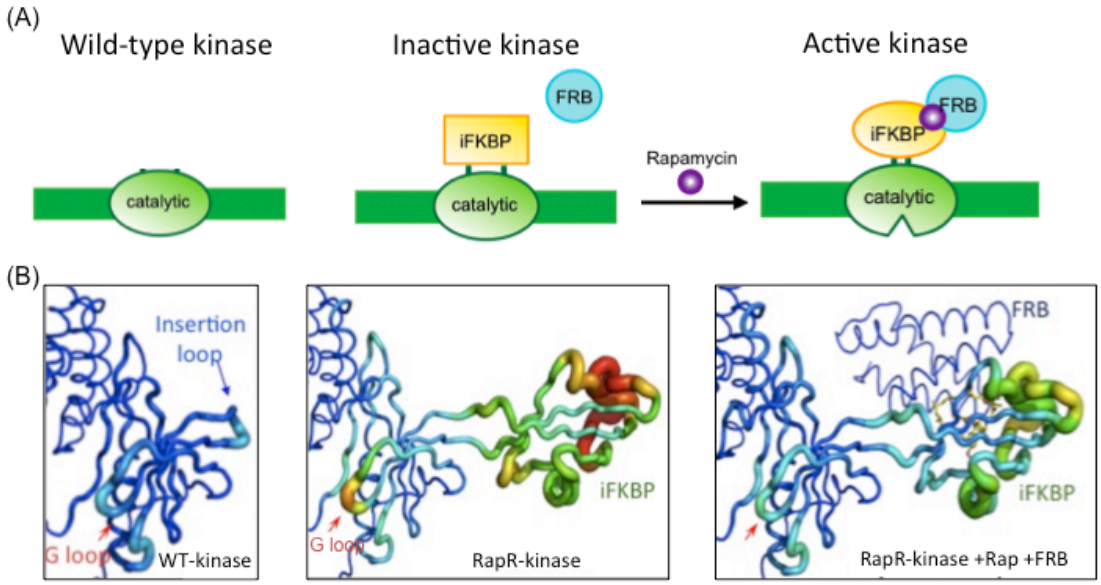

Figure 3.10. Design of RapR kinases.

(A) Schematic representation of the approach used to regulate the catalytic activity of kinases. A fragment of FKBP (iFKBP) is inserted into the catalytic domain, disrupting kinase activity. The binding of FRB to iFKBP, via rapamycin, restores activity. (B) Molecular dynamics simulations for the wild-type kinase and RapR-kinase indicate that the insertion of iFKBP increases the conformational fluctuation of the G-loop, greatly reducing kinase activity. The binding of FRB to iFKBP stabilizes the conformational dynamics of the G-loop,

thereby restoring kinase activity. Warmer color and thicker backbone indicate increasing of fluctuation. (Figure modified from Karginov *et al., Nat. Biotechnol*. 2010.)

To understand the mechanism by which the LOV domain is regulating kinase activity, we computationally analyzed a structural model of photosensitive Src kinase (PI-Src). The LOV domain was inserted into the insertion loop at the ATP binding site using a GPG linker. Using the discrete molecular dynamics (DMD) simulation (114), we analyzed the stability of the PI-Src fusion protein and evaluated the effect of light-induced unfolding of the LOV2 Jα-helix on the engineered kinase. The magnitude of the G-loop fluctuations in chimeric Src kinase, with two states of the LOV domain (the dark and lit states), were measured and compared to results from wild-type Src kinase (without the LOV insertion). A simulation of the lit state of PI-Src was created by inserting the LOV domain with an unfolded Jα-helix into Src, with constraints set up that prevented the refolding of the Jα-helix. The dark state of PI-Src corresponds to its native folded state and was recapitulated in DMD simulations without the need for additional constraints. Comparing root-mean-square fluctuations (RMSF) of the kinase backbones (Fig. 3.11), we observed that the differences in G-loop stability among the lit form of PI-Src, the dark form of PI-Src and wild-type Src are small. Unlike the simulations for RapR-kinase, the results from PI-Src simulations suggest that the possible mechanism of kinase activity regulation by the LOV domain is not based on modulation of G-loop dynamics.

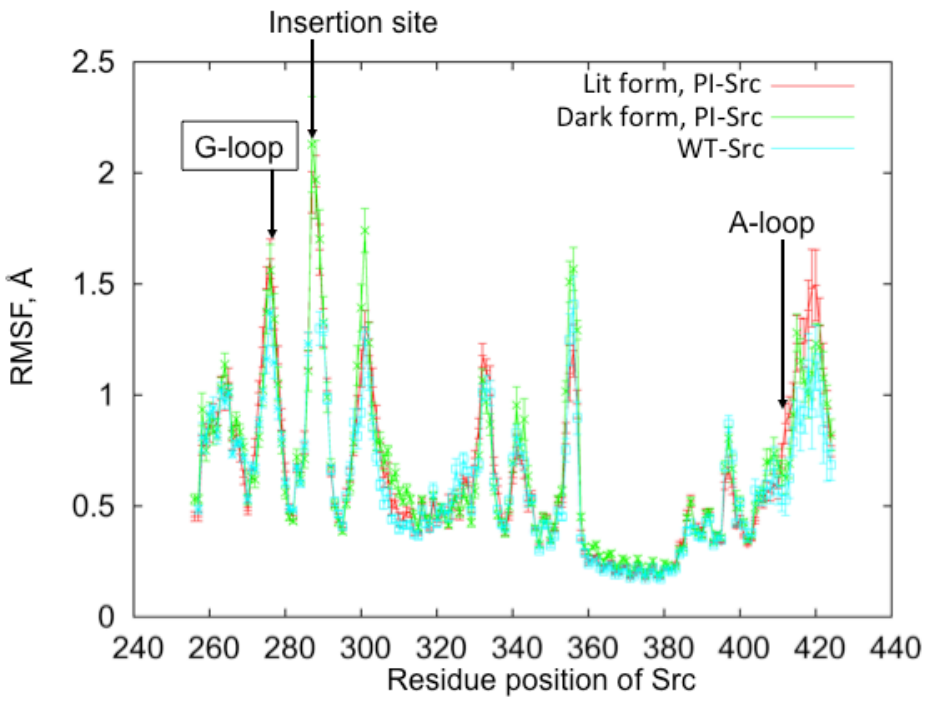

Figure 3.11. Root mean square fluctuations of the ATP binding site for the lit state of PI-Src, the dark state of PI-Src, and wild-type Src.

Root mean square fluctuation (RMSF) of each amino acid residue in the catalytic domain of Src. Red and green lines indicate the lit and dark forms of PI-Src. Wild-type Src is shown as a blue line. The x-axis represents the residue position of Src. G-loop (282-287), insertion loop (295-297), and A-loop (404-432).

Besides the stability of the G loop (64-66), the conformation of the ATP binding pocket is also critical for catalytic activity. The ATP binding pocket of Src kinase is located at the cleft between the N terminal and C terminal lobes of the catalytic domain (50, 116). The modulation of conformation and position of key components in this pocket, including the G-loop, αC helix, and A-loop, are essential for catalytic activity. Structures of active and inactive conformations have been characterized by X-ray crystallography. The A-loop acts as a gate to occlude substrate entry into the binding pocket in the inactive state. While in the

active state, the A-loop moves outward and opens up the binding pocket (47, 52, 57, 116, 117). To characterize the conformation of the ATP binding site, we sampled the pairwise distances between the alpha-carbon atoms of the pocket forming residues for the lit and dark states of PI-Src and wild-type Src. The differences of average inter-residue distances between these kinases were analyzed. Our simulation results revealed a large conformational change in the ATP-binding pocket between the dark and lit states of PI-Src, as shown in Fig. 3.12A. In the dark state, the binding site is open, as indicated by the distance between the A-loop and the β-sheet, similar to the binding site in wild-type Src. In the lit state, the distance between the A-loop and β-sheet decreases, mimicking the closed state of the binding site. Our results agree with previous structural studies, that the active form of Src has an open conformation of the ATP binding pocket (PDB:1Y57) and the inactive form of Src has a closed conformation of the ATP binding pocket (PDB:2SRC) (Fig. 3.12B). Based on our observations and simulations, we conclude that the PI-Src chimeric protein is active in the dark and inhibited by light (Fig. 3.12C).

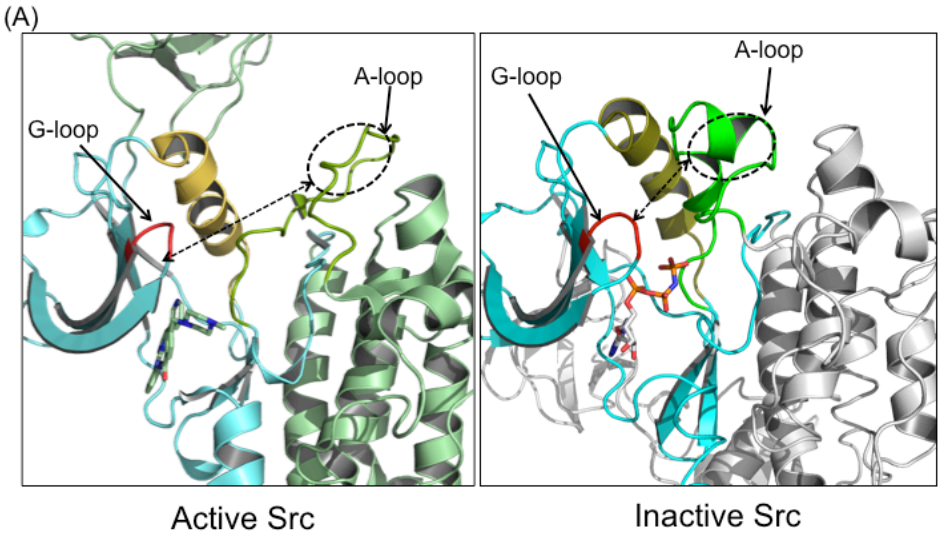

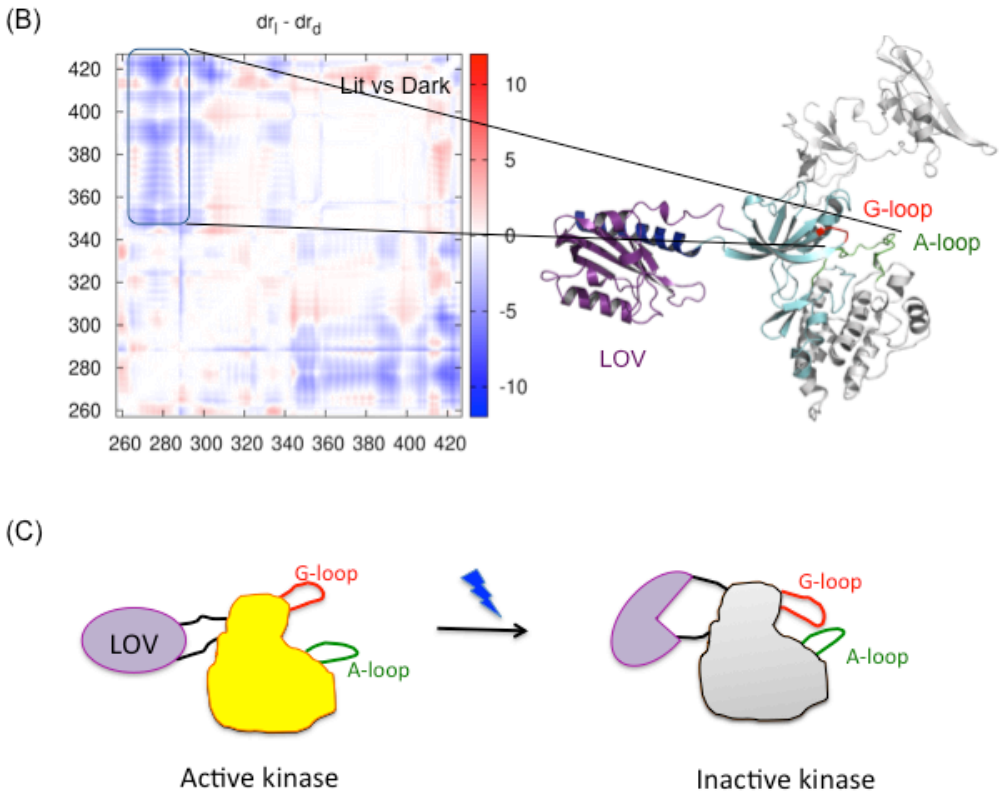

Figure 3.12. Model of light-regulated PI-Src activity.

(A) X-ray crystallographic structures of Src kinase in the active (left) and inactive (right) forms. In the active form, the A-loop is unfolded and shifted away from the G-loop and β-sheet. (B) Difference of inter-residue distances within the ATP binding site between the lit and dark states of the PI-Src kinase as analyzed by molecular dynamics simulation. In the diagram, positive changes in distance from the lit to the dark state are indicated by red color and negative changes are shown in blue. The boxed area in the figure corresponds to the residues of the A-loop (green) and the G-loop (red).

3.4 Materials and Methods

Antibodies and reagents

The following antibodies were used in these studies: anti-GFP antibody (Clontech), anti-phospho-Paxillin (Tyr31) antibody (Invitrogen). IgG-coupled agarose beads were purchased from Millipore and glutathione agarose beads were purchased from Pierce. All restriction enzymes were purchased from New England Biolabs.

Cell culture and transfection

293 LinXE and SYF (*src*$^{-/-}$ *yes*$^{-/-}$ *fyn*$^{-/-}$) cells were cultured in Dulbecco's Modified Eagle Medium (DMEM) supplemented with 1% GlutaMax™ (Invitrogen) and 10% FBS. Transient transfections were carried out using Fugene®6 reagent (Promega) in 293 LinXE cells following the manufacturer's protocol. For production of SYF cells stably incorporating the EGFP tagged Src and LOV-Src variants, a modified retroviral expression vector pBabe-sin-Puro-CMV was used. The vector was derived from pBabe-sin-Puro-tet-CMV by removing the tetracycline-response element. SYF cells were stably transduced using a retroviral system with the Src variants in pBabe vectors under the control of a CMV promoter. Cells were selected by puromycin (2 μg/ml) and FAC sorted for optimal expression.

Construction of LOV-Src fusion proteins

The LOV2 domain (Leu404- Leu547) of *Avena sativa* phototropin1 was used to generate LOV-Src fusion proteins. Wild-type, dark mutant (C450M), and lit mutant (I510E/I539E) LOV domains were used in this study. The LOV domain inserts were amplified by PCR such

that their 5'- and 3'-end sequences annealed at the insertion loop of Src with the desired linker. An overlap extension PCR cloning strategy was used to fuse LOV inserts into the Src gene without generating enzyme sites. The LOV inserts were inserted into Src by replacing its glycine 296 in the insertion loop. NotI/BamHI cutting sites were created using primers at the 5' and 3' ends of the LOV-Src-EGFP-Myc fusion proteins. The digested PCR fragments were then cloned into the pUSE plasmid. The linkers used in this study to insert the LOV domain into Src are listed as follows (left linker/right linker): G/G, GPG/GPG, and GSG/GSG. To generate constructs in a viral vector, Src and LOV-Src variants were amplified from pUSE constructs as a mega primer and inserted into the pBabe-sin-Puro-CMV vector using a method modified from the Stratagene Quickchange site-directed mutagenesis protocol.

***in vitro* kinase assay**

To assay the tyrosine kinase activity of Src variants, transient transfected 293 LinXE cells or SYF stable cell lines were grown in 6-well dishes under dark or light. Cells were washed with cold PBS and lysed in 300 μl of sample buffer. Cell lysates were boiled, resolved by SDS-PAGE and transferred to PVDF membranes. Western blots were blocked in 5% BSA or 5% nonfat dry milk in TBST (30 mM Tris, 150 mM NaCl, 0.5% Tween-20) and incubated in anti-phosphotyrosine antibody (4G10) to identify phosphorylated proteins, anti-GFP (JL-8) antibody to identify fluorescently tagged kinases and an anti-actin antibody was used as a loading control. Blots were washed followed by incubation with horseradish peroxidise (HRP)-conjungated secondary antibodies. The enhanced chemiluminescence substrate was

applied for 5 minutes to PVDF membranes and the proteins were visualized by exposing the blots to x-ray film.

Cell migration assay

Cell migration assays were developed by modifying methods described in *Nature Protocols* (118). SYF cells stably expressing Src derivatives were placed onto fibronectin-coated 96-well dishes for 12-18 h in darkness. A vertical line was generated using a p10 pipet tip in each well containing confluent cells. Cell debris was removed by washing the cells with PBS once and replacing with fresh medium. Cells were then returned to the tissue culture incubator with or without light treatment for 7 hours. Images were acquired using phase-contrast microscopy with an UPlan FL N Ph1 10X/0.3NA objective lens and the distances between the wound edges were analyzed using MetaMorph software. The migration rates were obtained from the wound width between 0h and 7h and expressed as migration distance over time (μm/min). For each sample we took four images along the scratch, and 5 readings of gap distance were measured from each of the images. Each experiment was repeated four times for each cell type. As a result, each Src derivative generated 80 readings for gap distance and was plotted as a box and whisker plot using IgorPro.

Time course of kinase activity

Myc-tagged Src kinases variants were expressed in 293 LinXE cells for 24 h in darkness. Cells were washed with cold PBS and lysed with lysis buffer (20 mM HEPES-KOH, pH 7.8, 50 mM KCl, 100 mM NaCl, 1mM EGTA, 1% NP40, 1mM NaF and 0.1 mM Na_3VO_4). Cell lysates were then clarified by centrifugation at 3,000 x g for 10 min at 4°C. The kinases were

then purified from cleared lysates by incubating anti-Myc antibody coated IgG-linked agarose beads with cell lysate for 2 h at 4 °C. The beads were washed two times with wash buffer (20 mM HEPES-KOH, pH 7.8, 50 mM KCl, 100 mM NaCl, 1mM EGTA, 1% NP40) and two times with kinase reaction buffer (25 mM HEPES, pH 7.5, 5 mM $MgCl_2$, 5 mM $MnCl_2$, 0.5 mM EGTA). The immunoprecipitates were suspended in kinase reaction buffer. All the procedures were handled in the dark room with red-light or covered with aluminum foil. Precipitates were aliquotted into 1.5-ml eppendorf tubes covered with aluminum foil and placed on ice under light illumination (full-spectrum 40W light bulb, samples were kept about 22-cm away from the light source). The aliquots were then exposed to light by sequentially unwrapping the aluminum foil for samples starting with the longest exposure time point. Kinase assays were carried out at room temperature under light illumination in the presence of ATP and the purified N-terminal fragment of paxillin as the substrate for 5 min. The reactions were stopped by adding 2X Laemmli protein sample buffer. The reaction mixture was then analyzed by western blot using an anti-GFP antibody to measure the levels of kinase protein and an anti-phospho-Paxillin antibody to measure the levels of phosphorylated substrates.

Live cell imaging

Cells for live cell imaging were placed on 2.5 μg/ml fibronectin coated coverslips 2 hr before imaging. Coverslips were mounted in a closed chamber filled with Leibovtiz's L15 medium (Invitrogen) containing 5% FBS and placed on a microscope stage with a heated stage adaptor. A 100W mercury arc lamp was used as the light source for global irradiation. The light was filtered through an ND 2.0 (1.0% transmission) filter and an EGFP excitation filter

(ET470/40 nm). The power of the light passing through the objective lens was measured using a power meter (Thorlabs), and found to be around 100 μW at 450 nm. The photo-cycle used in this experiment was 15 min off/30 min on/30 min off. Pulsed irradiation (5 s on/5 s off) was used to minimize cellular damage by the light. DIC images were acquired every 30 seconds using an Olympus IX81-ZDC microscope equipped with a CoolSNAP HQ2 14-bit camera (Photometrics).

CHAPTER FOUR: CONCLUSIONS AND FUTURE DIRECTIONS

4.1 Summary of Findings

Rapidly activated Src family protein analogs reveal isoform differences in generation of cell morphodynamics

The SFK family is comprised of nine homologous members. Their distinct expression patterns and cellular distributions imply that they have unique roles, but it has been difficult to identify the functions of individual family members; their highly similar structures enable them to compensate for one another after genetic manipulation, and have prevented production of specific inhibitors. As an important therapeutic target, many studies have been conducted to reveal the functions of individual Src family members in different aspects. However, only a few studies attempted to compare functions of Src isoforms in parallel due to the limitation of available tools (44,59,62,74). In my thesis project, I have developed novel tools based on the understanding of structure and regulation of Src family kinases to control activity of specific Src isoforms in living cells. The temporal regulation of each Src isoform, combined with the computational quantification methods for morphodynamics developed in this project, led to new insights about dynamic localization of kinases and the resulting cellular consequences. The main findings of this work are summarized below:

1. We demonstrated for the first time that activation of each Src isoform induced different cell morphological changes: activation of Fyn generated uniform spreading, while activation of Src initiated polarized movement. Activation of LynA induced long membrane projections with complex shapes, including sharp bends. Activation of Yes induced a phenotype similar to Src, but led to cell polarization at a much later time.
2. We developed a novel computational method, called *Squigglymorph*, to analyze cell morphodynamics induced by each kinase. The change in cell boundary at each successive pair of time points was represented as a single point on the 2D parameter space, resulting in a trajectory that showed the changing behavior of the cell over time. Critical parameter values used to define cell motion from the parameter space can be adjusted by users to accommodate different experimental needs.
3. Both Fyn and Src initially produced extensive spreading, but only for Src was this followed by polarized movement. Changing Fyn's lipidation to that of Src enabled Fyn to induce polarized movement, thereby revealing that aspects of isoform specific regulation depend on kinase localization.
4. Lipidiation is an important determinant of translocation to adhesions upon activation. Only kinases lacking palmitoylation (Src and Fyn $Palm^-$) moved to adhesions, and the timing of this movement paralleled release from the perinuclear compartment.

Development of photo-inhibition of Src

I successfully used the LOV domain to control kinase activity *in vivo*. Molecular dynamic simulation of changes in the Src ATP binding pocket suggested that the mechanisms regulating kinase activity are different between the LOV domain insertion and the iFKBP insertion approaches. Using cellular assays I demonstrated the inhibition of Src by light irradiation showed the cellular effects after ten minutes. The slow cellular effects resulting from inhibition of PI-Src may be due to the dephosphorylation kinetics. Hyperphosphorylated Src substrates must be dephosphorylated by the phosphatases in order to generate cellular responses.

4.2 Future directions

The remarkable advantages of the RapR kinase strategy includes gaining temporal control of each SFK's activity, enabling comparison of cellular responses before and after activation in the same cell *in vivo*, and providing biologically relevant information regarding kinase localization. Our results suggest that the major determinant for functional specificity of each SFK is cellular localization. Therefore, identification of substrates using RapR kinases, rather than assays of kinase-substrate interactions from cell lysates (44), provides unique insights about biologically relevant phsophorylation events. This approach enables activation of a specific kinase *in vivo*, allowing the kinases to interact with proper substrates in the same cellular compartments. The temporal control of kinase activity allows identifying the phosphorylation events stimulated solely from kinases, by comparing the phosphorylation profiles before and after induction. Proteomics experiments can be conducted to identify

substrates specific for each SFK. Furthermore, the timing of phosphorylation events can be correlated with the observed phenotypes to identify signaling pathways inducing the specific cellular responses.

One of the major concerns about the RapR strategy is the physiological relevance of the cellular consequences induced by these engineered kinases. A constitutively activating mutation, identified as tyrosine-530 for the human c-Src protein, was included in the engineered kinases to eliminate their intracellular regulation, so that their kinase activity would be solely under the control of rapamycin. However, the elevated SFK activities and expressions, but not the mutations on SFKs, were commonly found in human cancers. The levels of activity and expression of these engineered kinases should be compared to those of wild type kinases in parallel, proving that the distinct responses observed in this thesis were not due to exaggerated activation of the kinases. The activity of engineered kinases upon adding rapamycin is dose-dependent (63). Therefore the biologically relevant level of kinase activity can be achieved by using a suitable dosage of rapamycin or adjusting the expression level of the engineered kinases. Another approach to mimic biological conditions is to develop a rapamycin regulatable c-terminal Src kinase (CSK) and activate this kinase in cells expressing only one specific SFK. This can be achieved by using SYF cells expressing only one of the three wild type SFKs (Src, Fyn and Yes). Activation of CSK will elevate the SFK activity levels in a more biologically relevant manner.

Furthermore, among the multiple proteins regulating focal adhesion dynamics, focal adhesion kinase (FAK) and Src kinases have been shown to be important in regulating focal adhesion turnover (28, 119, 120). The finding that Fyn and Src differ in regulating focal adhesions upon activation opens a broad topic on SFKs and focal adhesion dynamics.

Previous studies suggest that site-specific tyrosine phosphorylation of FAK results in different effects in regulating FAK activity and in association with different lipid microdomains (121-123). Using RapR kinases specific for Fyn and Src will allow us to examine whether they regulate focal adhesion dynamics differently through site-specific tyrosine phosphorylation of FAK.

Because these engineered kinases regulated either by rapamycin or light were designed based on modifying the conserved domains in kinases, the modifications could be incorporated into other kinases, and potentially used as a general approach for many biological applications. Ideally, these approaches will be easily deployable without detailed structural information.

REFERENCES

1. Rous P (1911) A sarcoma of the fowl transmissible by an agent separable from the tumor cells. *J Exp Med* 13:397.

2. Rubin H (1955) Quantitative relations between causative virus and cell in the Rous no. 1 chicken sarcoma. *Virology* 1:445–473.

3. Martin GS (1970) Rous sarcoma virus: a function required for the maintenance of the transformed state. *Nature* 227:1021–1023.

4. Brugge JS, Erikson RL (1977) Identification of a transformation-specific antigen induced by an avian sarcoma virus. *Nature* 269:346–348.

5. Stehelin D, Fujita DJ, Padgett T, Varmus HE, Bishop JM (1977) Detection and enumeration of transformation-defective strains of avian sarcoma virus with molecular hybridization. *Virology* 76:675–684.

6. Purchio AF, Erikson E, Brugge JS, Erikson RL (1978) Identification of a polypeptide encoded by the avian sarcoma virus src gene. *Proc Natl Acad Sci USA* 75:1567–1571.

7. Levinson AD, Oppermann H, Levintow L, Varmus HE, Bishop JM (1978) Evidence that the transforming gene of avian sarcoma virus encodes a protein kinase associated with a phosphoprotein. *Cell* 15:561–572.

8. Czernilofsky AP et al. (1980) Nucleotide sequence of an avian sarcoma virus oncogene (src) and proposed amino acid sequence for gene product. *Nature* 287:198–203.

9. Shalloway D, Zelenetz AD, Cooper GM (1981) Molecular cloning and characterization of the chicken gene homologous to the transforming gene of Rous sarcoma virus. *Cell* 24:531–541.

10. Anderson SK, Gibbs CP, Tanaka A, Kung HJ, Fujita DJ (1985) Human cellular src gene: nucleotide sequence and derived amino acid sequence of the region coding for the carboxy-terminal two-thirds of pp60c-src. *Mol Cell Biol* 5:1122–1129.

11. Tanaka A et al. (1987) DNA sequence encoding the amino-terminal region of the human c-src protein: implications of sequence divergence among src-type kinase oncogenes. *Mol Cell Biol* 7:1978–1983.

12. Collett MS, Brugge JS, Erikson RL (1978) Characterization of a normal avian cell protein related to the avian sarcoma virus transforming gene product. *Cell* 15:1363–1369.

13. Collett MS, Erikson E, Purchio AF, Brugge JS, Erikson RL (1979) A normal cell protein similar in structure and function to the avian sarcoma virus transforming

gene product. *Proc Natl Acad Sci USA* 76:3159–3163.

14. Courtneidge SA, Levinson AD, Bishop JM (1980) The protein encoded by the transforming gene of avian sarcoma virus (pp60src) and a homologous protein in normal cells (pp60proto-src) are associated with the plasma membrane. *Proc Natl Acad Sci USA* 77:3783–3787.

15. Oppermann H, Levinson AD, Varmus HE, Levintow L, Bishop JM (1979) Uninfected vertebrate cells contain a protein that is closely related to the product of the avian sarcoma virus transforming gene (src). *Proc Natl Acad Sci USA* 76:1804–1808.

16. Brugge JS et al. (1979) Detection of the viral sarcoma gene product in cells infected with various strains of avian sarcoma virus and of a related protein in uninfected chicken cells. *J Virol* 29:1196–1203.

17. Stehelin D, Varmus HE, Bishop JM, Vogt PK (1976) DNA related to the transforming gene(s) of avian sarcoma viruses is present in normal avian DNA. *Nature* 260:170–173.

18. Takeya T, Hanafusa H (1982) DNA sequence of the viral and cellular src gene of chickens. II. Comparison of the src genes of two strains of avian sarcoma virus and of the cellular homolog. *J Virol* 44:12–18.

19. Talamonti MS, Roh MS, Curley SA, Gallick GE (1993) Increase in activity and level of pp60c-src in progressive stages of human colorectal cancer. *J Clin Invest* 91:53–60.

20. Iravani S et al. (1998) Elevated c-Src protein expression is an early event in colonic neoplasia. *Lab Invest* 78:365–371.

21. Irby RB, Yeatman TJ (2000) Role of Src expression and activation in human cancer. *Oncogene* 19:5636–5642.

22. Ishizawar R, Parsons SJ (2004) c-Src and cooperating partners in human cancer. *Cancer Cell* 6:209–214.

23. Thomas SM, Brugge JS (1997) Cellular functions regulated by Src family kinases. *Annu Rev Cell Dev Biol* 13:513–609.

24. Shalloway D, Johnson PJ, Freed EO, Coulter D, Flood WA (1987) Transformation of NIH 3T3 cells by cotransfection with c-src and nuclear oncogenes. *Mol Cell Biol* 7:3582–3590.

25. Yamaguchi H, Wyckoff J, Condeelis J (2005) Cell migration in tumors. *Current Opinion in Cell Biology* 17:559–564.

26. Avizienyte E et al. (2002) Src-induced de-regulation of E-cadherin in colon cancer

cells requires integrin signalling. *Nat Cell Biol* 4:632–638.

27. Webb DJ, Parsons JT, Horwitz AF (2002) Adhesion assembly, disassembly and turnover in migrating cells -- over and over and over again. *Nat Cell Biol* 4:E97–100.

28. Webb DJ et al. (2004) FAK-Src signalling through paxillin, ERK and MLCK regulates adhesion disassembly. *Nat Cell Biol* 6:154–161.

29. Noritake H, Miyamori H, Goto C, Seiki M, Sato H (1999) Overexpression of tissue inhibitor of matrix metalloproteinases-1 (TIMP-1) in metastatic MDCK cells transformed by v-src. *Clin Exp Metastasis* 17:105–110.

30. Linder S, Wiesner C, Himmel M (2011) Degrading devices: invadosomes in proteolytic cell invasion. *Annu Rev Cell Dev Biol* 27:185–211.

31. Eliceiri BP et al. (1999) Selective requirement for Src kinases during VEGF-induced angiogenesis and vascular permeability. *Mol Cell* 4:915–924.

32. Playford MP, Schaller MD (2004) The interplay between Src and integrins in normal and tumor biology. *Oncogene* 23:7928–7946.

33. Yeatman TJ (2004) A renaissance for SRC. *Nat Rev Cancer* 4:470–480.

34. Martin GS (2004) The road to Src. *Oncogene* 23:7910–7917.

35. Weisberg E, Manley PW, Cowan-Jacob SW, Hochhaus A, Griffin JD (2007) Second generation inhibitors of BCR-ABL for the treatment of imatinib-resistant chronic myeloid leukaemia. *Nat Rev Cancer* 7:345–356.

36. Stein PL, Vogel H, Soriano P (1994) Combined deficiencies of Src, Fyn, and Yes tyrosine kinases in mutant mice. *Genes Dev* 8:1999–2007.

37. Roche S, Fumagalli S, Courtneidge SA (1995) Requirement for Src family protein tyrosine kinases in G2 for fibroblast cell division. *Science* 269:1567–1569.

38. Posadas EM et al. (2009) FYN is overexpressed in human prostate cancer. *BJU Int* 103:171–177.

39. Chen Z-Y et al. (2010) Roles of Fyn in pancreatic cancer metastasis. *J Gastroenterol Hepatol* 25:293–301.

40. Han NM, Curley SA, Gallick GE (1996) Differential activation of pp60(c-src) and pp62(c-yes) in human colorectal carcinoma liver metastases. *Clin Cancer Res* 2:1397–1404.

41. Stettner MR et al. (2005) Lyn kinase activity is the predominant cellular SRC kinase activity in glioblastoma tumor cells. *Cancer Res* 65:5535–5543.

42. Shah K, Liu Y, Deirmengian C, Shokat KM (1997) Engineering unnatural nucleotide specificity for Rous sarcoma virus tyrosine kinase to uniquely label its direct substrates. *Proc Natl Acad Sci USA* 94:3565–3570.

43. Ulrich SM, Kenski DM, Shokat KM (2003) Engineering a "methionine clamp" into Src family kinases enhances specificity toward unnatural ATP analogues. *Biochemistry* 42:7915–7921.

44. Takeda H et al. (2010) Comparative analysis of human SRC-family kinase substrate specificity in vitro. *J Proteome Res* 9:5982–5993.

45. Brady G, Williams RL, Nordström K, Vennström B, Iscove NN (1988) A selectable temperature-sensitive v-src Moloney retrovirus. *Oncogene* 3:687–689.

46. Qiao Y, Molina H, Pandey A, Zhang J, Cole PA (2006) Chemical rescue of a mutant enzyme in living cells. *Science* 311:1293–1297.

47. Xu W, Doshi A, Lei M, Eck MJ, Harrison SC (1999) Crystal structures of c-Src reveal features of its autoinhibitory mechanism. *Mol Cell* 3:629–638.

48. Resh MD (1994) Myristylation and palmitylation of Src family members: the fats of the matter. *Cell* 76:411–413.

49. Pérez Y et al. (2013) Lipid binding by the Unique and SH3 domains of c-Src suggests a new regulatory mechanism. *Sci Rep* 3:1295.

50. Xu W, Harrison SC, Eck MJ (1997) Three-dimensional structure of the tyrosine kinase c-Src. *Nature* 385:595–602.

51. Williams JC, Wierenga RK, Saraste M (1998) Insights into Src kinase functions: structural comparisons. *Trends in Biochemical Sciences* 23:179–184.

52. Sicheri F, Kuriyan J (1997) Structures of Src-family tyrosine kinases. *Curr Opin Struct Biol* 7:777–785.

53. Young MA, Gonfloni S, Superti-Furga G, Roux B, Kuriyan J (2001) Dynamic coupling between the SH2 and SH3 domains of c-Src and Hck underlies their inactivation by C-terminal tyrosine phosphorylation. *Cell* 105:115–126.

54. Tatosyan AG, Mizenina OA (2000) Kinases of the Src family: structure and functions. *Biochemistry Mosc* 65:49–58.

55. Roskoski R (2004) Src protein-tyrosine kinase structure and regulation. *Biochem Biophys Res Commun* 324:1155–1164.

56. Boggon TJ, Eck MJ (2004) Structure and regulation of Src family kinases. *Oncogene* 23:7918–7927.

57. Cowan-Jacob SW et al. (2005) The crystal structure of a c-Src complex in an active conformation suggests possible steps in c-Src activation. *Structure* 13:861–871.

58. Frame MC (2004) Newest findings on the oldest oncogene; how activated src does it. *J Cell Sci* 117:989–998.

59. Klinghoffer RA, Sachsenmaier C, Cooper JA, Soriano P (1999) Src family kinases are required for integrin but not R signal transduction. *EMBO J* 18:2459–2471.

60. Fincham V et al. (1994) Functions of the v-Src protein tyrosine kinase. *Cell Biol Int* 18:337–344.

61. Oneyama C, Hikita T, Nada S, Okada M (2008) Functional dissection of transformation by c-Src and v-Src. *Genes Cells* 13:1–12.

62. Oneyama C et al. (2009) Transforming potential of Src family kinases is limited by the cholesterol-enriched membrane microdomain. *Mol Cell Biol* 29:6462–6472.

63. Karginov AV, Ding F, Kota P, Dokholyan NV, Hahn KM (2010) Engineered allosteric activation of kinases in living cells. *Nat Biotechnol* 28:743–747.

64. Grant BD, Hemmer W, Tsigelny I, Adams JA, Taylor SS (1998) Kinetic analyses of mutations in the glycine-rich loop of cAMP-dependent protein kinase. *Biochemistry* 37:7708–7715.

65. Taylor SS, Radzio-Andzelm E (1994) Three protein kinase structures define a common motif. *Structure* 2:345–355.

66. Wong L, Jennings PA, Adams JA (2004) Communication pathways between the nucleotide pocket and distal regulatory sites in protein kinases. *Acc Chem Res* 37:304–311.

67. Barouch-Bentov R et al. (2009) A conserved salt bridge in the G loop of multiple protein kinases is important for catalysis and for in vivo Lyn function. *Mol Cell* 33:43–52.

68. Koch CA, Anderson D, Moran MF, Ellis C, Pawson T (1991) SH2 and SH3 domains: elements that control interactions of cytoplasmic signaling proteins. *Science* 252:668–674.

69. Pawson T, Gish GD (1992) SH2 and SH3 domains: from structure to function. *Cell* 71:359–362.

70. Songyang Z, Cantley LC (1995) Recognition and specificity in protein tyrosine kinase-mediated signalling. *Trends in Biochemical Sciences* 20:470–475.

71. Waksman G, Kuriyan J (2004) *Structure and specificity of the SH2 domain.*

72. Weng Z et al. (1994) Identification of Src, Fyn, and Lyn SH3-binding proteins: implications for a function of SH3 domains. *Mol Cell Biol* 14:4509–4521.

73. Summy JM, Guappone AC, Sudol M, Flynn DC (2000) The SH3 and SH2 domains are capable of directing specificity in protein interactions between the non-receptor tyrosine kinases cSrc and cYes. *Oncogene* 19:155–160.

74. Summy JM et al. (2003) The SH4-Unique-SH3-SH2 domains dictate specificity in signaling that differentiate c-Yes from c-Src. *J Cell Sci* 116:2585–2598.

75. Koegl M, Zlatkine P, Ley SC, Courtneidge SA, Magee AI (1994) Palmitoylation of multiple Src-family kinases at a homologous N-terminal motif. *Biochem J* 303 (Pt 3):749–753.

76. Wolven A, Okamura H, Rosenblatt Y, Resh MD (1997) Palmitoylation of p59fyn is reversible and sufficient for plasma membrane association. *Mol Biol Cell* 8:1159–1173.

77. Alland L, Peseckis SM, Atherton RE, Berthiaume L, Resh MD (1994) Dual myristylation and palmitylation of Src family member p59fyn affects subcellular localization. *J Biol Chem* 269:16701–16705.

78. Sandilands E, Brunton VG, Frame MC (2007) The membrane targeting and spatial activation of Src, Yes and Fyn is influenced by palmitoylation and distinct RhoB/RhoD endosome requirements. *J Cell Sci* 120:2555–2564.

79. Kasahara K et al. (2007) Rapid trafficking of c-Src, a non-palmitoylated Src-family kinase, between the plasma membrane and late endosomes/lysosomes. *Exp Cell Res* 313:2651–2666.

80. Dunn GA (1983) Characterising a kinesis response: time averaged measures of cell speed and directional persistence. *Agents Actions Suppl* 12:14–33.

81. Othmer HG, Dunbar SR, Alt W (1988) Models of dispersal in biological systems. *J Math Biol* 26:263–298.

82. Petrie RJ, Doyle AD, Yamada KM (2009) Random versus directionally persistent cell migration. *Nat Rev Mol Cell Biol* 10:538–549.

83. Wadsworth P (1999) Regional regulation of microtubule dynamics in polarized, motile cells. *Cell Motil Cytoskeleton* 42:48–59.

84. Glasgow JE, Daniele RP (1994) Role of microtubules in random cell migration: stabilization of cell polarity. *Cell Motil Cytoskeleton* 27:88–96.

85. Gundersen GG, Cook TA (1999) Microtubules and signal transduction. *Current Opinion in Cell Biology* 11:81–94.

86. Etienne-Manneville S (2004) Actin and microtubules in cell motility: which one is in control? *Traffic* 5:470–477.

87. Lippincott-Schwartz J, Roberts TH, Hirschberg K (2000) Secretory protein trafficking and organelle dynamics in living cells. *Annu Rev Cell Dev Biol* 16:557–589.

88. Schmoranzer J, Simon SM (2003) Role of microtubules in fusion of post-Golgi vesicles to the plasma membrane. *Mol Biol Cell* 14:1558–1569.

89. Sheetz MP, Felsenfeld D, Galbraith CG, Choquet D (1999) Cell migration as a five-step cycle. *Biochem Soc Symp* 65:233–243.

90. Volberg T, Romer L, Zamir E, Geiger B (2001) pp60(c-src) and related tyrosine kinases: a role in the assembly and reorganization of matrix adhesions. *J Cell Sci* 114:2279–2289.

91. Ridley AJ et al. (2003) Cell migration: integrating signals from front to back. *Science* 302:1704–1709.

92. Wozniak MA, Modzelewska K, Kwong L, Keely PJ (2004) Focal adhesion regulation of cell behavior. *Biochim Biophys Acta* 1692:103–119.

93. Timpson P, Jones GE, Frame MC, Brunton VG (2001) Coordination of cell polarization and migration by the Rho family GTPases requires Src tyrosine kinase activity. *Curr Biol* 11:1836–1846.

94. Frame MC, Fincham VJ, Carragher NO, Wyke JA (2002) v-Src's hold over actin and cell adhesions. *Nat Rev Mol Cell Biol* 3:233–245.

95. Li L, Okura M, Imamoto A (2002) Focal adhesions require catalytic activity of Src family kinases to mediate integrin-matrix adhesion. *Mol Cell Biol* 22:1203–1217.

96. Berginski ME, Vitriol EA, Hahn KM, Gomez SM (2011) High-resolution quantification of focal adhesion spatiotemporal dynamics in living cells. *PLoS ONE* 6:e22025.

97. Kasahara K et al. (2004) Trafficking of Lyn through the Golgi caveolin involves the charged residues on alphaE and alphaI helices in the kinase domain. *J Cell Biol* 165:641–652.

98. Sato I et al. (2009) Differential trafficking of Src, Lyn, Yes and Fyn is specified by the state of palmitoylation in the SH4 domain. *J Cell Sci* 122:965–975.

99. Ikeda K et al. (2009) Requirement of the SH4 and tyrosine-kinase domains but not the kinase activity of Lyn for its biosynthetic targeting to caveolin-positive Golgi membranes. *Biochim Biophys Acta* 1790:1345–1352.

100. Karginov AV, Hahn KM (2011) Allosteric activation of kinases: design and application of RapR kinases. *Curr Protoc Cell Biol* Chapter 14:Unit 14.13.

101. Briggs WR, Christie JM (2002) Phototropins 1 and 2: versatile plant blue-light receptors. *Trends Plant Sci* 7:204–210.

102. Christie JM (2007) Phototropin blue-light receptors. *Annu Rev Plant Biol* 58:21–45.

103. Swartz TE et al. (2001) The photocycle of a flavin-binding domain of the blue light photoreceptor phototropin. *J Biol Chem* 276:36493–36500.

104. Harper SM, Neil LC, Gardner KH (2003) Structural basis of a phototropin light switch. *Science* 301:1541–1544.

105. Zoltowski BD, Vaccaro B, Crane BR (2009) Mechanism-based tuning of a LOV domain photoreceptor. *Nat Chem Biol* 5:827–834.

106. Strickland D, Moffat K, Sosnick TR (2008) Light-activated DNA binding in a designed allosteric protein. *Proc Natl Acad Sci USA* 105:10709–10714.

107. Wu YI et al. (2009) A genetically encoded photoactivatable Rac controls the motility of living cells. *Nature* 461:104–108.

108. Lee J et al. (2008) Surface sites for engineering allosteric control in proteins. *Science* 322:438–442.

109. Salomon M et al. (2001) An optomechanical transducer in the blue light receptor phototropin from Avena sativa. *Proc Natl Acad Sci USA* 98:12357–12361.

110. Westhoff MA, Serrels B, Fincham VJ, Frame MC, Carragher NO (2004) SRC-mediated phosphorylation of focal adhesion kinase couples actin and adhesion dynamics to survival signaling. *Mol Cell Biol* 24:8113–8133.

111. Hanke JH et al. (1996) Discovery of a novel, potent, and Src family-selective tyrosine kinase inhibitor. Study of Lck- and FynT-dependent T cell activation. *J Biol Chem* 271:695–701.

112. Brandvold KR, Steffey ME, Fox CC, Soellner MB (2012) Development of a highly selective c-Src kinase inhibitor. *ACS Chem Biol* 7:1393–1398.

113. Ding F, Dokholyan NV (2008) Dynamical roles of metal ions and the disulfide bond in Cu, Zn superoxide dismutase folding and aggregation. *Proc Natl Acad Sci USA* 105:19696–19701.

114. Ding F, Tsao D, Nie H, Dokholyan NV (2008) Ab initio folding of proteins with all-atom discrete molecular dynamics. *Structure* 16:1010–1018.

115. Karginov AV, Ding F, Kota P, Dokholyan NV, Hahn KM (2010) Engineered

allosteric activation of kinases in living cells. *Nat Biotechnol* 28:743.

116. Yamaguchi H, Hendrickson WA (1996) Structural basis for activation of human lymphocyte kinase Lck upon tyrosine phosphorylation. *Nature* 384:484–489.

117. Breitenlechner CB et al. (2005) Crystal structures of active SRC kinase domain complexes. *J Mol Biol* 353:222–231.

118. Liang C-C, Park AY, Guan J-L (2007) In vitro scratch assay: a convenient and inexpensive method for analysis of cell migration in vitro. *Nat Protoc* 2:329–333.

119. Schaller MD, Hildebrand JD, Parsons JT (1999) Complex formation with focal adhesion kinase: A mechanism to regulate activity and subcellular localization of Src kinases. *Mol Biol Cell* 10:3489–3505.

120. Brunton VG et al. (2005) Identification of Src-specific phosphorylation site on focal adhesion kinase: dissection of the role of Src SH2 and catalytic functions and their consequences for tumor cell behavior. *Cancer Res* 65:1335–1342.

121. Lim Y et al. (2007) Focal adhesion kinase is negatively regulated by phosphorylation at tyrosine 407. *J. Biol Chem* 282:10398-10404

122. Baillat G, Siret C, Delamarre E, Luis J (2008) Early adhesion induces interaction of FAK and Fyn in lipid domains and activates raft-dependent Akt signaling in SW480 colon cancer cells. *Biochim Biophys Acta* 1783:2323–2331.

123. Deramaudt TB et al. (2011) FAK phosphorylation at Tyr-925 regulates cross-talk between focal adhesion turnover and cell protrusion. *Mol Biol Cell* 22:964–975.